AD-A066 177 NAVAL RESEARCH LAB WASHINGTON D C F/G 20/5
FREE ELECTRON LASERS AND STIMULATED SCATTERING FROM RELATIVISTI--ETC(U)
DEC 78 P SPRANGLE, R A SMITH, V L GRANATSTEIN

UNCLASSIFIED NRL-MR-3911 SBIE-AD-E000 269 NL

1 OF 1
AD
A066 177

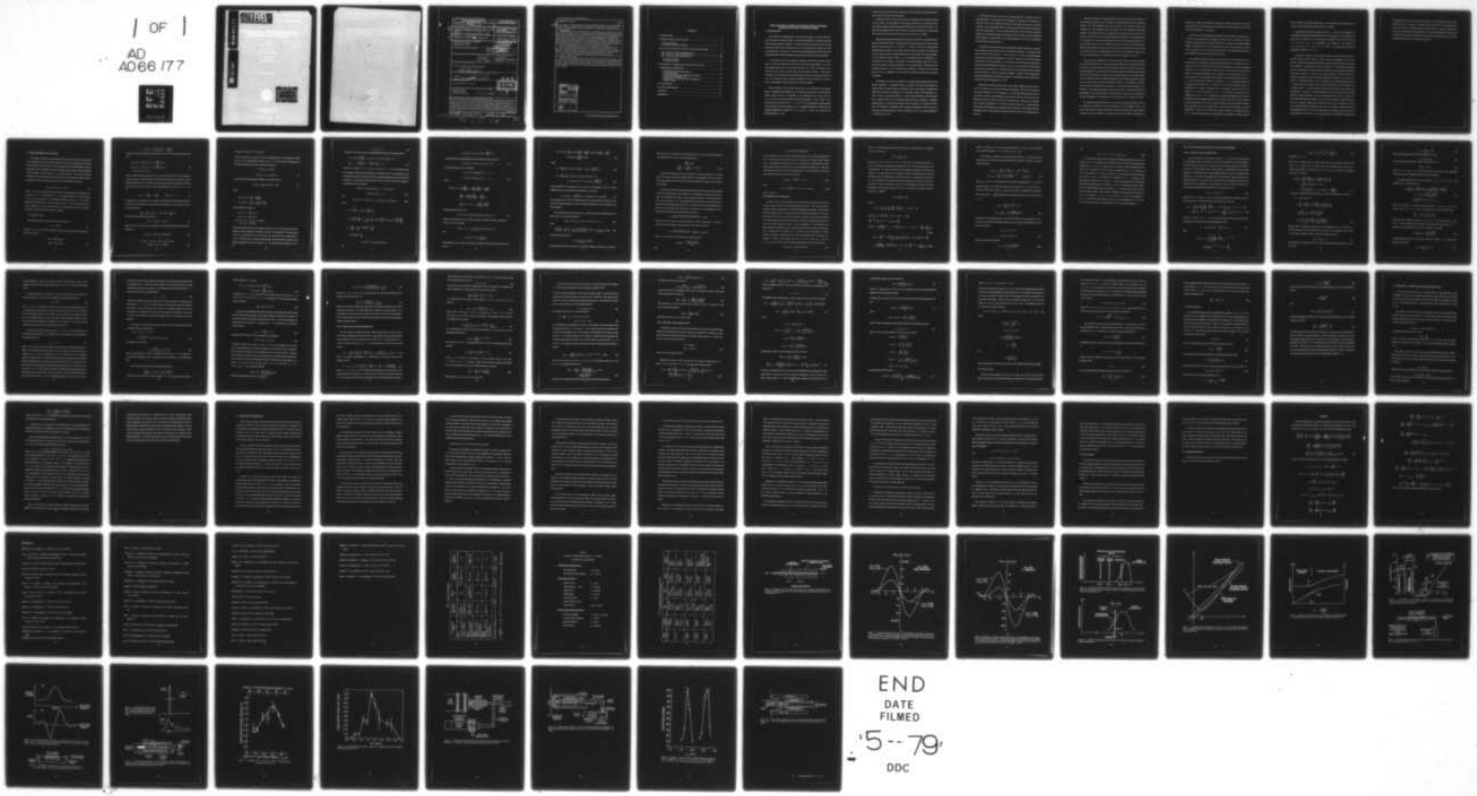

END
DATE
FILMED
5-79
DDC

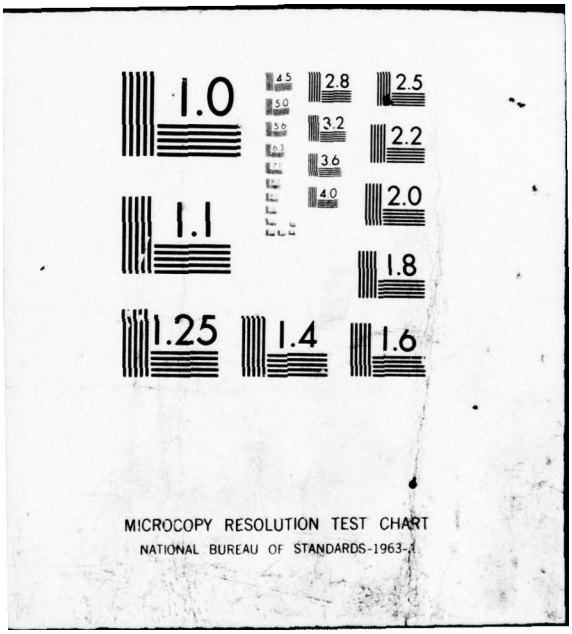
1.0
1.1
1.25
1.4
1.6
1.8
2.0
2.2
2.5
2.8
3.2
3.6
4.0
4.5
5.0
5.6
MICROCOPY RESOLUTION TEST CHART
NATIONAL BUREAU OF STANDARDS-1963-A

AD A066177

DDC FILE COPY

(12) NW LEVEL III

[redacted]

[redacted]

[redacted]

[redacted]

[redacted]

[redacted]

[redacted]

[redacted]

[redacted]

[redacted]

[redacted]

DDC
RECEIVED
MAR 22 1979
B

[redacted]

[redacted]

[redacted]

[redacted]

[redacted]

[redacted]

[redacted]

[redacted]

[redacted]

[redacted]

[redacted]

NRL Memorandum Report 3913

Free Electron Lasers and Stimulated Scattering from Relativistic Electron Beams

P. Sprangle

Plasma Physics Division

Robert A. Smith

Sigma Research, Inc.

V. L. Granatstein

Plasma Physics Division

December 8, 1978

NAVAL RESEARCH LABORATORY
Washington, D.C.

Approved for public release; distribution unlimited

SECURITY CLASSIFICATION OF THIS PAGE (When Data Entered)

REPORT DOCUMENTATION PAGE

READ INSTRUCTIONS BEFORE COMPLETING FORM

1. REPORT NUMBER (14) NRL-MR-
NRL Memorandum Report 3911

2. GOVT ACCESSION NO.

3. RECIPIENT'S CATALOG NUMBER

4. TITLE (and Subtitle) (6)
FREE ELECTRON LASERS AND STIMULATED SCATTERING FROM RELATIVISTIC ELECTRON BEAMS

5. TYPE OF REPORT & PERIOD COVERED (9)
Interim report on a continuing NRL problem

6. PERFORMING ORG. REPORT NUMBER

7. AUTHOR(s) (10)
P. Sprangle, Robert A. Smith, [redacted] V. L. Granatstein

8. CONTRACT OR GRANT NUMBER(s) (16) RR011109

9. PERFORMING ORGANIZATION NAME AND ADDRESS
Naval Research Laboratory
Washington, D.C. 20375

10. PROGRAM ELEMENT, PROJECT, TASK AREA & WORK UNIT NUMBERS
NRL Problem H02-47
Subtask RR0110941 (17)

11. CONTROLLING OFFICE NAME AND ADDRESS (11) 8

12. REPORT DATE
December [redacted] 1978

13. NUMBER OF PAGES
74

14. MONITORING AGENCY NAME & ADDRESS (if different from Controlling Office) (12) 75 p.

15. SECURITY CLASS. (of this report)
UNCLASSIFIED

15a. DECLASSIFICATION/DOWNGRADING SCHEDULE

16. DISTRIBUTION STATEMENT (of this Report)

Approved for public release; distribution unlimited.

(18) SBIE

17. DISTRIBUTION STATEMENT (of the abstract entered in Block 20, if different from Report)

(19) AD-E000 269

DDC
RECEIVED
MAR 22 1979
B

18. SUPPLEMENTARY NOTES

*Jaycor, Alexandria, VA 22304

19. KEY WORDS (Continue on reverse side if necessary and identify by block number)
Free electron lasers
Stimulated scattering
Relativistic electron beams
beta(sub z0)c.
K sub 0;

20. ABSTRACT (Continue on reverse side if necessary and identify by block number)

Free electron lasers based on stimulated scattering from relativistic electron beams show potential for a new class of coherent radiation sources ranging from millimeter wavelengths down to optical wavelengths and beyond which are characterized by continuous tunability, very high power levels and competitive efficiencies. Here we present a comprehensive fully-relativistic treatment of stimulated backscattering from an electron beam with streaming velocity $\beta_{z0}c$. The incident pump wave is taken to be a static, circularly polarized, periodic magnetic field with wavenumber k_0; the frequency of the scattered radiation is $\beta_{z0}ck_0/(1-\beta_{z0})$. The analysis is linear in the scattered wave fields, but contains the pump

(Continued)

DD FORM 1 JAN 73 1473 EDITION OF 1 NOV 65 IS OBSOLETE S/N 0102-014-6601

251 950

SECURITY CLASSIFICATION OF THIS PAGE (When Data Entered)

(beta(sub z0)cK(sub 0)/((1-beta(sub z0)).

79 01 31 058

20. ABSTRACT (Continued)

field to all orders. The physical mechanism of the backscattering is provided by the $\mathbf{v} \times \mathbf{B}$ ponderomotive forces acting on the beam electrons in the presence of both the pump and the scattered waves. This force produces a longitudinal charge bunching which in turn gives rise to source currents for the scattered waves.

The analysis is steady state but spatially bounded. In addition to the ponderomotive force, other effects which are incorporated are the self-consistent collective scalar potential, and free-streaming terms which arise from boundary conditions. Various regimes of the interaction may be distinguished according to which of these effects are dominant; *viz.*, (1) a low gain, single particle regime appropriate to tenuous cold beams, in which the boundary terms lead to spatial transients; (2) a high-gain, single-particle regime of a tenuous thermal beam, (stimulated Compton scattering); (3) a high-gain cold beam regime. This last regime is subdivided into; (a) a weak-pump limit, in which the longitudinal density wave satisfies normal-mode dispersion and the collective scalar potential dominates the ponderomotive potential; and (b) a strong-pump limit, in which the ponderomotive force dominates.

From a heuristic argument based on the fact that the saturation mechanism for each of these processes is the trapping of the beam electrons in the potential wells of the longitudinal wave, we estimate the saturated amplitude of the backscattered wave and the efficiency of energy extraction from the beam. In addition, we find the integrated gain over the system length for the spatially transient case (1), and the exponentiation length in the spatially homogeneous cases (2) and (3a,b).

Finally, we discuss the present status of experimental work both with linear accelerators and with intense relativistic electron beams.

Agreement between experimental results and the predictions of the linear theory in regimes 1 and 3a is good. The other regimes have not yet been subjected to experiment and no definitive experimental test of the nonlinear theory has been made in any regime. Theoretical efficiencies are largest for case 3b, and we present sample calculations of gigawatt lasers with 11% efficiency at a wavelength of 1700 μm and 0.25% efficiency at 0.58 μm. Possible techniques for substantially improving on these efficiencies are also discussed.

ACCESSION for
NTIS White Section
DDC Buff Section
UNANNOUNCED
JUSTIFICATION
BY
DISTRIBUTION/AVAILABILITY CODES
Dist. AVAIL. and/or SPECIAL
A

CONTENTS

I. INTRODUCTION 1

II. PHYSICAL MODEL AND ANALYSIS 8

(a) General Formalism 8
(b) Evaluation of the Current Density 15

III. GAIN AND SATURATION LEVEL IN VARIOUS FEL REGIMES 19

Case 1. Low Gain, Tenuous-Cold-Beam Limit 19
Case 2. High Gain, Tenuous-Thermal-Beam Limit 25
Case 3. High Gain, Dense-Cold-Beam Limit 28

(a) Weak-pump regime 31
(b) Strong-pump regime 33

IV. DISCUSSION: A VISIBLE-LIGHT FREE ELECTRON LASER 35

V. LABORATORY EXPERIMENTS 38

(a) Experiments in the low-gain regime at infrared wavelengths 40
(b) Submillimeter generation in the high-gain, collective regime with electromagnetic pump 42
(c) Experiments in the high-gain, collective regime with a magnetic wiggler 44

VI. CONCLUSIONS 46

VII. ACKNOWLEDGMENTS 47

APPENDIX 48

REFERENCES 50

FREE ELECTRON LASERS AND STIMULATED SCATTERING FROM RELATIVISTIC ELECTRON BEAMS

I. INTRODUCTION

The possibility of developing lasers in which the active medium is a stream of free electrons has recently evoked much interest. The potential advantages are numerous and include both continuous frequency tunability (*e.g.* through the variation of electron energy) and very high power operation, since no damage can occur to the lasing medium as happens with liquid or solid-state lasers. Furthermore, it is hoped that the high efficiencies which characterize free electron generators of microwave radiation can eventually be realized with free electron lasers.

In the past few years, the first operation of high peak power free electron lasers has been reported. They have generated seven kilowatts in the infrared regime (Deacon *et al.*, 1977) and megawatt power levels in the infrared (Granatstein *et al.*, 1977). Furthermore, recent theoretical results indicate that much larger powers should be achievable. The operative mechanism in these experiments was stimulated backscattering of a low frequency pump wave from a relativistic electron beam, leading to amplification of coherent radiation at a high frequency corresponding to a double doppler shift of the pump frequency.

The low frequency pump wave may take the form of a static spatially periodic magnetic field or a propagating electromagnetic wave. In the case that the pump wave is a static periodic magnetic field of period l, the frequency of the backscattered wave will be given by $(1 + v_z/c)\gamma_z^2 v_z(2\pi/l)$, which for a highly relativistic beam becomes $\sim 4\pi\gamma_z^2 c/l$ where v_z is the axial velocity of the electrons and $\gamma_z = (1 - v_z^2/c^2)^{-1/2}$. If the pump field is an electromagnetic pump at frequency ω_o and wavenumber $k_o = \omega_o/c$, propagating antiparallel to the electrons, the upshifted backscattered frequency will be $(1 + v_z/c)^2\gamma_z^2\omega_o \simeq 4\gamma_z^2\omega_o$. For either type of

Manuscript submitted Nov. 14, 1978.

incident pump wave the scattered wave frequency can be varied simply by changing the electron beam energy or the incident pump wavelength.

Stimulated scattering of photons by an electron ensemble was first predicted by Kapitza and Dirac (1933). The first analyses of high frequency radiation from a relativistic electron beam passing through a periodic magnetic field (undulator) was made by Motz (1951). The proposal for generating short wavelength radiation by stimulated scattering of an electromagnetic pump wave from a relativistic electron beam is due to Pantell *et al.* (1968).

Experiments demonstrating stimulated scattering with an output in the infrared have been carried out at Stanford University. These experiments utilize the relatively low current electron beam in a linear accelerator ($I \simeq 1A$, $24\,MV < V < 43\,MV$). They are in the single-particle scattering regime and hence do not involve collective electron oscillations. The single pass gain is low and the process is strongly dependent on the finite length of the interaction region. The first Stanford experiment (Elias *et al.*, 1976) demonstrated wave amplification at a wavelength of 10.6 μm using a static periodic 2.4 kG helical magnetic pump with a 3.2 cm period; a 7% increase in power was achieved in a 5.2 m interaction length. The second Stanford experiment (Deacon *et al.*, 1977) produced laser oscillations in an optical cavity with peak power of 7 kW at a wavelength of 3.4 μm; 0.01% of the electron beam energy was converted into radiation.

The analysis by Motz (1951) is applicable to the single-particle scattering process in the Stanford experiments. A subsequent analysis by Sukhatme and Wolff (1973) included the important effect of the finite length of the interaction region. The treatment of Sukhatme and Wolff (1973) was quantum mechanical, as were analyses by Madey (1971) and Madey *et al.* (1973). However, recent analyses (Hopf *et al.*, 1976a; Kroll and McMullin, 1978) have shown that a classical treatment of the stimulated scattering process is appropriate. Additional, detailed analyses of the Stanford experiments have also appeared in the literature (Colson, 1976, 1977; Bernstein and Hirshfield, 1978; Sprangle and Granatstein, 1978), as have considerations of extending operation to shorter wavelengths up to the x-ray regime (Hasegawa *et al.*, 1976; Elias *et al.*, 1976).

With intense relativistic electron beams, collective effects play an important role in the scattering process. The theoretical analyses (Sprangle and Granatstein, 1974; Sprangle *et al.*, 1975) show that for intense magnetized relativistic electron beams, the pump wave may decay into either a space charge beam mode or a cyclotron beam mode depending on, among other things, the pump frequency. The axial magnetic field can be used to increase the effective strength of the pump field by adjusting the electron cyclotron frequency to equal roughly the pump frequency in the beam frame. The resonance produced in this way can substantially enhance the gain of the scattered wave.

Experimental and theoretical research demonstrating stimulated scattering in the submillimeter regime have been carried out at the Naval Research Laboratory. In experiments using intense relativistic electron beams ($I \sim 30\ kA$, $1\ MV < V < 3\ MV$), strong submillimeter radiation was first reported by Granatstein *et al.* (1974). Analyses of this process by Sprangle and Granatstein (1974) and Sprangle *et al.* (1975) show that the submillimeter radiation was generated by stimulated Raman-type scattering. That is, one of the scattered waves was a beam space charge wave enhanced by a resonance between the pump frequency and the electron cyclotron frequency. A followup experiment designed to enhance the stimulated Raman scattering process generated a megawatt of radiation in a superradiant oscillator operating at a wavelength of 400 μm (Granatstein *et al.*, 1977).

Experiments at Columbia University using a static, rippled, magnetic-field pump with outputs in the centimeter wave regime (Efthimion and Schlesinger, 1977) and in the millimeter wave regime (Marshal *et al.*, 1977; Gilgenbach *et al.*, 1978) clearly distinguished between the cases where the idler was a space-charge mode and where the idler was a beam cyclotron mode. Efficiencies as large as 0.2% were measured in these experiments. Recently a joint Columbia-NRL experiment (McDermott *et al.*, 1978) has reported operation of a stimulated Raman scattering laser which employs a quasi-optical cavity; laser output was 1 MW at 400 μm and line narrowing to $\Delta\omega/\omega = 2\%$ was observed (compared with $\Delta\omega/\omega \gtrsim 10\%$ in the superradiant oscillator case).

Theoretical treatments of stimulated Raman scattering in plasma were first applied to laser-pellet fusion studies as well as to ionospheric experiments (Silin, 1965, 1967; DuBois and Goldman, 1965, 1967; Nishikawa, 1968; Kaw and Dawson, 1971; Perkins and Kaw, 1971; Forslund *et al.*, 1973; Manheimer and Ott, 1974; Drake *et al.*, 1974). Relativistic analyses with application to the generation of short wavelength radiation using electron beams are now in the literature, treating both the linear regime (Sprangle and Granatstein, 1974; Miroshnichenko, 1975; Sprangle *et al.*, 1975; Kroll and McMullin, 1978) and the non-linear regime (Kwan *et al.*, 1977; Sprangle and Drobot, 1978). Efficiencies greater than 10% have been calculated, but no efficiency approaching this level has been measured to date; experiments have not been driven into saturation. However, e-folding lengths on the order of ten centimeters have been calculated and correspond closely to experimental measurements (Granatstein *et al.*, 1977).

The present paper confines itself to free electron lasers based on stimulated scattering from relativistic electron beams. Other mechanisms involving relativistic electron beams which may lead to free electron lasers have also been studied. While none of these has to date produced the high power in the submillimeter and infrared regimes that characterize the stimulated scattering work, the research is in much too early a stage to ignore the other possible mechanisms. For reference we cite the following mechanisms which have been considered as the basis for free electron sources of coherent high frequency radiation: (1) interaction of a relativistic electron beam with periodic slow wave structures or with dielectric media (Coleman, 1961; Walsh *et al.*, 1977; Schneider and Spitzer, 1974; Gover and Yariv, 1978); and (2) scattering of electromagnetic waves from the front of a relativistic electron beam or from a moving ionization front (Granatstein *et al.*, 1976; Pasour *et al.*, 1977; Buzzi *et al.*, 1977; Lampe *et al.*, 1978).

The linear regime has been discussed in a survey by Granatstein and Sprangle (1977) and in comprehensive treatments by Kroll and McMullin (1977) and Hasegawa (1977). The present paper presents an original reformulation of stimuated scattering theory that attempts to encompass all previous treatments, and compares the theory with available experimental data.

In addition, we present a semi-qualitative discussion of non-linear saturation. Also, the linear treatment differs from previous analyses by performing a perturbation expansion about an exact electron beam equilibrium in a general way.

The details of the physical mechanism associated with FELs depend, to some extent, on the type of scattering process under consideration, which in turn is a function of the system parameters, such as beam energy, temperature and density, the length of the interaction region, strength of pump field, *etc.* There are characteristics of the physical mechanism, however, which are common to all the various scattering processes. These common characteristics can best be described classically in the beam frame of reference.

In the following discussion, quantities in the beam frame will be written with primes. In the beam frame we stipulate that the existing electron equilibrium is perturbed by a low frequency density wave; the existence of this wave will be justified later. Only waves propagating along the z axis, *i.e.*, the direction of the beam velocity in the laboratory frame, will be considered. This longitudinal perturbation has a frequency and wavenumber given by (ω', k'). The introduction of a large-amplitude high-frequency incident electromagnetic pump, E_o', at (ω_o', k_o') forces the electrons to oscillate at a frequency $\omega_o' >> \omega'$ in the direction along E_o' with a maximum velocity given by $v_{o\perp}' = |e|E_o'/(m_o\omega_o')$. This transverse oscillation velocity $v_{o\perp}'$, perpendicular to k_o', couples to the density wave, thus inducing a transverse current at frequency $\omega_+' = \omega' + \omega_o'$ and wave number $k_+' = k' + k_o'$. This current now generates an electromagnetic wave at (ω_+', k_+'). The generated or scattered electromagnetic field consists of backscattered waves propagating antiparallel to the incident pump wave. Forward scattered waves are also induced, but will not be considered because they are downshifted in frequency when transformed back to the laboratory frame. The pump and backscattered wave couple through the $\mathbf{v}' \times \mathbf{B}'$ term in the Lorentz force equation, resulting in a longitudinal force at (ω', k'). This induced longitudinal force, also called the ponderomotive or radiation pressure

force, will reinforce the original longitudinal wave. The backscattered electromagnetic wave is, therefore, unstable resulting in stimulated emission of radiation.

The ponderomotive potential associated with the (ω, k) wave, may be comparable to or may dominate the self space charge potential wave set up by the beam. If the frequency of the pump wave is far above any of the characteristic frequencies of the beam we find that $\omega_o' = -ck_o'$ and $\omega_+' = ck_+'$. The backscattered wave frequency in the laboratory is $\omega_+ = \gamma_z(\omega_o' + v_z k_o') = (1 + v_z/c)\gamma_z\omega_o' = (1 + v_z/c)^2\gamma_z^2\omega_o$. For a highly relativistic beam the backscattered frequency is $\omega_+ \approx 4\gamma_z^2\omega_o$.

In Section II we discuss in detail the physical model to be analyzed, which consists of a relativistic electron beam of arbitrary intensity entering and propagating through a static, periodic, circularly polarized magnetic pump field. The general analytic formalism is presented. The calculation is relativistically covariant and consists of a Vlasov-Maxwell perturbation analysis. The perturbation is performed about an exact electron beam equilibrium distribution, formed from constants of the motion in the magnetic pump field. The general analysis culminates in expressions for the driving current densities which, through the wave equations, are sources of the backscattered fields. The time dependences of the scattered fields are harmonic, *i.e.*, temporal steady state conditions exist. Spatial transient effects due to the boundary of the interaction region at $z = 0$ are retained by choosing the scattered fields to have an arbitrary spatial dependence. In Section III we obtain spatial growth rates and estimates for the saturation efficiencies and field amplitudes of various scattering processes: Case (1) is a transient, low-gain, single-particle regime and applies to the recent FEL experiments at Stanford University; Case (2) is a high-gain, single-particle, thermal-beam regime, which is equivalent to the well known stimulated Compton scattering process; Case (3a) is a high-gain, cold beam, weak pump scattering regime where collective space charge effects play a dominant role; Case (3b) is the strong pump limit of Case (3a). In Case (3b) collective space charge effects are dominated by

the ponderomotive forces. The experiments performed at the Naval Research Laboratory and Columbia University correspond to the regime covered by Case (3a). These processes have been listed in order of increasing interaction strength. Section IV contains a discussion and illustrates an example which applies to generation of coherent visible radiation. Section V gives a description of the pertinent experimental work, and conclusions regarding future work, both experimental and theoretical, are presented in Section VI.

II. PHYSICAL MODEL AND ANALYSIS

We consider a completely non-neutralized electron beam, the motion of which is treated fully relativistically. Only spatial variations along the z axis will be considered for the electron beam, pump field and scattered fields. The scattered fields consist of electromagnetic as well as electrostatic waves. The amplitude of the static magnetic pump is taken to increase adiabatically in space, reaching a constant value for $z > 0$, as shown in figure 1. The reason for including this feature in our model will become clear when the form for the equilibrium electron distribution function is chosen. We choose as the pump wave a magnetic field of the form

$$\mathbf{B}_o = B_o(\hat{e}_x \cos k_o z + \hat{e}_y \sin k_o z) \tag{1}$$

where $k_o = 2\pi/l$ and l is the period of the static field. The pump amplitude is considered to be a function of z for $z < 0$ and constant for $z > 0$. Although the field in (1) does not satisfy $\nabla \times \mathbf{B}_o = 0$, we may consider it to be a good approximation near the axis $r = 0$ of the exact helically symmetric field that is curl-free and varies as $I_o(k_o r)$. If the beam radius is taken to be much smaller then $l/2\pi$, the actual field can be well represented by (1). In our model the self electric and magnetic fields of the beam are neglected.

a) General Formalism

The pump field in Eq. (1) is derived from the vector potential

$$\mathbf{A}_o = -\mathbf{B}_o/k_o \tag{2}$$

where $\mathbf{B}_o = \nabla \times \mathbf{A}_o$. The steady state equations of motion for the relativistic beam particles in the field of Eq. (2) are

$$\begin{aligned} \partial p_x/\partial z &= \frac{|e|}{c}\,\partial A_{ox}/\partial z, \\ \partial p_y/\partial z &= \frac{|e|}{c}\,\partial A_{oy}/\partial z, \end{aligned} \tag{3}$$

$$p_z\, \partial p_z/\partial z = -\frac{|e|}{c}\left[p_x \frac{\partial A_{ox}}{\partial z} + p_y \frac{\partial A_{oy}}{\partial z}\right].$$

Equations (3) yield the following three constants of the motion for the individual beam particles:

$$\begin{aligned}
\alpha(p_x,z) &= p_x - \frac{|e|}{c} A_{ox}(z) = p_x + \frac{|e|B_o}{ck_o} \cos k_o z; \\
\beta(p_y,z) &= p_y - \frac{|e|}{c} A_{oy}(z) = p_y + \frac{|e|B_o}{ck_o} \sin k_o z; \\
u(\mathbf{p}) &= (p_x^2 + p_y^2 + p_z^2)^{1/2};
\end{aligned} \tag{4}$$

where α and β are the canonical momenta in the x and y directions and u is the magnitude of the total momentum. These constants of the motion will be used later to construct the equilibrium distribution function. The electric and magnetic fields of the scattered waves are denoted by $\mathbf{E}(z,t)$ and $\mathbf{B}(z,t)$ and are given in terms of the potentials $\phi(z,t)$ and $\mathbf{A}(z,t) = (A_x, A_y, 0)$ by

$$\mathbf{E}(z,t) = -\frac{\partial \phi}{\partial z}\hat{e}_z - \frac{1}{c}\frac{\partial \mathbf{A}}{\partial t}; \qquad \mathbf{B}(z,t) = \nabla \times \mathbf{A}. \tag{5}$$

We shall perform a perturbation Vlasov analysis by expanding the electron distribution function to first order in the potentials ϕ and $\mathbf{A}$, about the exact equilibrium. The relativistic form for the Vlasov equation is

$$\frac{\partial f}{\partial t} + v_z \frac{\partial f}{\partial z} - |e|(\mathbf{E} + \mathbf{v} \times (\mathbf{B}_o + \mathbf{B})/c) \cdot \frac{\partial f}{\partial \mathbf{p}} = 0.$$

The electron distribution function is written as

$$f(\mathbf{p},z,t) = f^{(0)}(\mathbf{p},z) + f^{(1)}(\mathbf{p},z,t), \tag{6}$$

where $f^{(0)}$ and $f^{(1)}$ are solutions of the equilibrium and first-order-perturbed Vlasov equations, respectively:

$$v_z\, \partial f^{(0)}/\partial z - \frac{|e|}{c}\, \mathbf{v} \times \mathbf{B}_o \cdot \partial f^{(0)}/\partial \mathbf{p} = 0; \tag{7a}$$

$$\begin{aligned}
&\partial f^{(1)}/\partial t + v_z\, \partial f^{(1)}/\partial z - \frac{|e|}{c}\, \mathbf{v} \times \mathbf{B}_o \cdot \partial f^{(1)}/\partial \mathbf{p} \\
&\quad = |e|(\mathbf{E} + \mathbf{v} \times \mathbf{B}/c) \cdot \partial f^{(0)}/\partial \mathbf{p};
\end{aligned} \tag{7b}$$

where $\mathbf{p} = \gamma m_o \mathbf{v}$ and $\gamma = (1 + p^2/m_o^2c^2)^{1/2}$.

It proves convenient at this point to make a transformation from the independent variables (p_x,p_y,p_z,z,t) to new independent variables (α, β, u, z, t). Thus we write the equilibrium and first order components of the electron distribution function as

$$g^{(0)}(\alpha,\beta,u) = f^{(0)}(\mathbf{p},z),$$

$$g^{(1)}(\alpha, \beta, u, z, t) = f^{(1)}(\mathbf{p}, z, t). \tag{8}$$

In terms of these new independent variables, Eq (7b) takes the form

$$\partial g^{(1)}/\partial t + \frac{p_z}{\gamma m_o} \partial g^{(1)}/\partial z = \mathbf{F} \cdot \mathbf{L}\, g^{(0)} \tag{9}$$

where

$$\mathbf{F}(\alpha,\beta,u,z,t) = |e| \left[\mathbf{E} + \frac{\mathbf{p} \times \mathbf{B}}{\gamma m_o c}\right]$$

$$\mathbf{L}\,(\alpha,\beta,u,z) = \hat{e}_x \frac{\partial}{\partial \alpha} + \hat{e}_y \frac{\partial}{\partial \beta} + \frac{\mathbf{p}}{u} \frac{\partial}{\partial u}$$

and the dependent variables are

$$p_x(\alpha, z) = \alpha + \frac{|e|}{c} A_{ox}(z),$$

$$p_y(\beta, z) = \beta + \frac{|e|}{c} A_{oy}(z),$$

$$p_z(\alpha,\beta, u, z) = [u^2 - p_x^2(\alpha,z) - p_y^2(\beta,z)]^{1/2}$$

$$\gamma(u) = (1 + u^2/m_o^2c^2)^{1/2}.$$

Note that the positive branch of the dependent variable $p_z(\alpha,\beta,u,z)$ will be chosen in order to represent a beam propagating in the positive z direction. The advantage of the transformation in Eq. (4) is clearly seen in Eq. (9), in which the Lorentz force term, corresponding to $\mathbf{v} \times \mathbf{B}_o \cdot \partial f^{(1)}/\partial \mathbf{p}$ in Eq. (7b), has been transformed away. We also exploit the symmetry of the model by transforming to the vector basis $(\hat{e}_+, \hat{e}_-, \hat{e}_z)$, which is given in terms of $(\hat{e}_x, \hat{e}_y, \hat{e}_z)$ by

$$\hat{e}_{\pm} = \frac{1}{2}\,(\hat{e}_x \pm i\,\hat{e}_y). \tag{10}$$

Noting Eq. (5) we may now write the scattered fields **E** and **B** in the interaction region as

$$\mathbf{E}(z,t) = \left[-\frac{1}{2}\,\frac{\partial\tilde{\phi}(z)}{\partial z}\,\hat{e}_z + i\frac{\omega}{c}\,\tilde{A}_+(z)\hat{e}_+ + i\frac{\omega}{c}\,\tilde{A}_-(z)\hat{e}_-\right]e^{-i\omega t}+c.c.,$$

$$\mathbf{B}(z,t) = -\,i\left[\frac{\partial\tilde{A}_+(z)}{\partial z}\,\hat{e}_+ - \frac{\partial\tilde{A}_-(z)}{\partial z}\,\hat{e}_-\right]e^{-i\omega t} + c.c., \tag{11}$$

where $\phi(z,t) = \frac{1}{2}\tilde{\phi}(z)e^{-i\omega t} + c.c.$, $\mathbf{A}_{\pm}(z,t) = \tilde{A}_{\pm}(z)\hat{e}_{\pm}e^{-i\omega t} + c.c.$ and c.c. denotes the complex conjugate. The chosen time dependence of the fields in Eqs. (11) is appropriate after all the temporal transients have decayed away and the spatial dependence along the z axis has been left arbitrary. In this new basis representation the force vector **F** and the vector operator **L** introduced in Eq. (9) take the form

$$\mathbf{F}(\alpha,\beta,u,z,t) = \tilde{F}_+(\alpha,\beta,u,z)e^{i\omega t}\,\hat{e}_+ + \tilde{F}_-(\alpha,\beta,u,z)e^{i\omega t}\hat{e}_-$$

$$+ \tilde{F}_z(\alpha,\beta,u,z)e^{i\omega t}\hat{e}_z \quad + c.c. \tag{12a}$$

and

$$\mathbf{L}(\alpha,\beta,u,z) = L_+(\alpha,\beta,u,z)\hat{e}_+ + L_-(\alpha,\beta,u,z)\hat{e}_- + L_z(\alpha,\beta,u,z)\hat{e}_z, \tag{12b}$$

where

$$\tilde{F}_{\pm} = \frac{|e|}{c}\left[i\omega - v_z(\alpha,\beta,u,z)\,\frac{\partial}{\partial z}\right]\tilde{A}_{\pm}(z),$$

$$\tilde{F}_z = \frac{|e|}{2}\left[-\frac{\partial\tilde{\phi}(z)}{\partial z} + \frac{1}{\gamma(u)m_o c}\left[p_-(\alpha,\beta,z)\,\frac{\partial\tilde{A}_+(z)}{\partial z} + p_+(\alpha,\beta,z)\,\frac{\partial\tilde{A}_-(z)}{\partial z}\right]\right],$$

$$L_{\pm} = \left[\frac{\partial}{\partial\alpha} \mp i\frac{\partial}{\partial\beta} + \frac{p_{\pm}(\alpha,\beta,z)}{u}\,\frac{\partial}{\partial u}\right],$$

$$L_z = \frac{p_z(\alpha,\beta,u,z)}{u}\,\frac{\partial}{\partial u},$$

$$v_z(\alpha,\beta,u,z) = p_z(\alpha,\beta,u,z)/(\gamma(u)m_o),$$

and

$$p_{\pm}(\alpha,\beta,z) = p_x \mp i p_y = \alpha \mp i\beta - \frac{|e|B_o}{ck_o} e^{\mp ik_o z}.$$

The perturbed part of the distribution function may also be written in the form

$$g^{(1)}(\alpha, \beta, u, z, t) = \tilde{g}^{(1)}(\alpha, \beta, u, z) e^{-i\omega t} + c.c. \tag{13}$$

The Vlasov equation for $g^{(1)}$ now becomes

$$(-i\omega + v_z(\alpha,\beta,u,z)\partial/\partial z)\,\tilde{g}^{(1)} e^{-i\omega t} \quad + c.c.$$

$$= \mathbf{F}\cdot\mathbf{L}\, g^{(0)} = \tilde{H}(\alpha,\beta,u,z) e^{-i\omega t} \quad + c.c., \tag{14}$$

where

$$\tilde{H}(\alpha, \beta, u, z) = \frac{|e|}{2c}\left[\left\{\left\{\left(i\omega - v_z \frac{\partial}{\partial z}\right)\tilde{A}_+\right\}\left(\frac{\partial}{\partial\alpha} + i\frac{\partial}{\partial\beta}\right)g^{(0)}\right.\right.$$

$$+ \left\{\left(i\omega - v_z \frac{\partial}{\partial z}\right)\tilde{A}_-\right\}\left(\frac{\partial}{\partial\alpha} - i\frac{\partial}{\partial\beta}\right)g^{(0)}$$

$$\left.\left. + \left\{i\omega(p_-\tilde{A}_+ + p_+\tilde{A}_-) - cp_z\frac{\partial\tilde{\phi}}{\partial z}\right\}\frac{1}{u}\frac{\partial g^{(0)}}{\partial u}\right],$$

The general solution of Eq. (14) is

$$\tilde{g}^{(1)}(\alpha, \beta, u, z) = \int_0^z dz'\, M(\alpha,\beta,u,z,z')\, \tilde{H}(\alpha, \beta, u, z'), \tag{15}$$

where we have assumed that the beam entered the interaction region unperturbed, *i.e.*, $\tilde{g}^{(1)}(\alpha, \beta, u, 0) = 0$, and where

$$M(\alpha, \beta, u, z, z') = \frac{1}{v_z(\alpha,\beta,u,z')} \exp(i\omega\tau(\alpha,\beta,u,z,z'))$$

and

$$\tau(\alpha,\beta,u,z,z') = \int_{z'}^{z} \frac{dz''}{v_z(\alpha,\beta,u,z'')}.$$

Rearranging Eq. (15), we may write the Fourier coefficient of the perturbed distribution function as

$$\tilde{g}^{(1)}(\alpha,\beta,u,z) = \left[\tilde{G}_+(\alpha,\beta,u,z)\left(\frac{\partial}{\partial\alpha} + i\frac{\partial}{\partial\beta}\right) + \tilde{G}_-(\alpha,\beta,u,z)\left(\frac{\partial}{\partial\alpha} - i\frac{\partial}{\partial\beta}\right) + \tilde{G}_z(\alpha,\beta,u,z)\frac{\partial}{\partial u}\right] g^{(0)}(\alpha,\beta,u) \tag{16}$$

where

$$\tilde{G}_\pm = \frac{|e|}{2c}\int_0^z dz'\, M(\alpha,\beta,u,z,z')\left(i\omega - v_z(\alpha,\beta,u,z')\frac{\partial}{\partial z'}\right)\tilde{A}_\pm(z'), \tag{17a}$$

$$\tilde{G}_z = \frac{|e|}{2c}\frac{1}{u}\int_0^z dz'\, M(\alpha,\beta,u,z,z')\left[i\omega p_-(\alpha,\beta,z')\,\tilde{A}_+(z') + i\omega p_+(\alpha,\beta,z')\,\tilde{A}_-(z') - cp_z(\alpha,\beta,u,z')\frac{\partial\tilde{\phi}(z')}{\partial z'}\right]. \tag{17b}$$

Careful inspection of the definition of $\tilde{G}_\pm$ shows that the integrand in (17a) is a perfect differential; thus, we can perform the integration over z' and obtain

$$\tilde{G}_\pm(\alpha,\beta,u,z) = \frac{-|e|}{2c}\left\{\tilde{A}_\pm(z) - \tilde{A}_\pm(0)\exp(i\omega\tau(\alpha,\beta,u,z,0))\right\}. \tag{18}$$

The expression in Eq. (15) for $\tilde{g}^{(1)}$ determines the first order perturbation of the electron distribution by the scattered fields with arbitrary axial space dependence, correct to all orders in the pump amplitude.

The perturbing driving current density $\mathbf{J}(z,t)$ which excites the scattered fields can be found from $g^{(1)}$ and is written in general as

$$\mathbf{J}(z,t) = [\tilde{J}_+(z)\,\hat{e}_+ + \tilde{J}_-(z)\hat{e}_- + \tilde{J}_z(z)\,\hat{e}_z]\,e^{-i\omega t} + c.c., \tag{19}$$

where

$$\begin{bmatrix}\tilde{J}_\pm(z)\\ \tilde{J}_z(z)\end{bmatrix} = \frac{-|e|}{m_o}\int_0^\infty \frac{1}{\gamma(u)}\begin{bmatrix}p_\pm(\alpha,\beta,z)\\ p_z(\alpha,\beta,u,z)\end{bmatrix}\tilde{g}^{(1)}(\alpha,\beta,u,z)\,\frac{u}{p_z(\alpha,\beta,u,z)}\,d\alpha d\beta du \tag{20}$$

and we have used the fact that

$$d^3p = \frac{u}{p_z(\alpha,\beta,u,z)}\,d\alpha d\beta du.$$

The general framework of the formalism is completed by relating self-consistently the scattered

fields in Eqs. (11) to the driving current density given by Eq. (19). This is done through the wave equations for $\phi(z,t)$ and $\mathbf{A}_{\pm}(z,t)$ which are given by

$$\frac{\partial^2 \phi}{\partial t \partial z} = 4\pi J_z,$$

$$\left\{\frac{\partial^2}{\partial z^2} - \frac{1}{c^2}\frac{\partial^2}{\partial t^2}\right\}\mathbf{A}_{\pm} = \frac{-4\pi}{c}\mathbf{J}_{\pm}. \qquad (21a,b)$$

It should be mentioned at this point that the terms $\tilde{G}_{\pm}$ which contribute to $g^{(1)}$ and thus to $\mathbf{J}$ do not appear in any previous analyses on FELs to our knowledge. This is due to the fact the previous analyses do not use the exact equilibrium distribution function in their treatment of the problem.

As already mentioned, the ponderomotive potential wave which results from the coupling of the pump and scattered wave is responsible for the longitudinal bunching of the beam electrons. The modulated beam together with the pump field produces a current density which drives the scattered wave. The most straightforward way to appreciate the bunching process associated with the ponderomotive potential is to consider the form of the Hamiltonian for a particle in the combined fields of the pump and scattered waves. The Hamiltonian of such a particle with zero transverse canonical momentum is given by

$$H = \sqrt{c^2 p_z^2 + |e|^2 (\mathbf{A}_o(z) + \mathbf{A}(z,t))^2 + m_o^2 c^4} - |e|\,\phi(z,t)$$

where $\mathbf{A}_o(z)$, $\mathbf{A}(z,t)$ and $\phi(z,t)$ are found from Eqs. (2) and (5). Since $|\mathbf{A}(z,t)| << |\mathbf{A}_o(z)|$ we can expand the Hamiltonian to first order in $\mathbf{A}(z,t)$ and write it in the form

$$H = \sqrt{c^2 p_z^2 + |e|^2 \mathbf{A}_o^2(z) + m_o^2 c^4} - |e|\left\{\phi(z,t) + \phi_{pond}(z,t)\right\}$$

where $\phi_{pond}(z,t)$ is defined as the ponderomotive potential, given by

$$\phi_{pond}(z,t) = -\frac{|e|\mathbf{A}_o(z)\cdot\mathbf{A}(z,t)}{\gamma m_o c^2},$$

and

$$\gamma = \sqrt{1 + p_z^2/m_o^2c^2 + |e|^2A_o^2/(m_o^2c^4)}.$$

In this expanded form we see that the transverse component of the scattered field given by $\mathbf{A}(z,t)$, when coupled to the pump field, plays a role similar to that of the space charge potential $\phi(z,t)$. The ponderomotive potential $\phi_{pond}(z,t)$, has the effect of axially bunching the beam. This bunching process in turn gives rise to the space charge scalar potential $\phi(z,t)$. Hence, the ponderomotive potential drives the space charge potential. For future reference, we note that the ponderomotive potential can be put into the form

$$\phi_{pond}(z,t) = \frac{\tilde{\phi}_{pond}(z)}{2}\, e^{-i\omega t} + c.c., \tag{22a}$$

where

$$\tilde{\phi}_{pond}(z) = \frac{2\Omega_o}{\gamma c k_o}\left\{e^{ik_o z}\,\tilde{A}_+(z) + e^{-ik_o z}\,\tilde{A}_-(z)\right\} \tag{22b}$$

and $\Omega_o = |e|B_o/m_oc$.

(b) Evaluation of the Current Density

In order to obtain an explicit expression for the driving current density given in Eq. (19) we need to specify a form for the equilibrium distribution function. As was mentioned earlier, the pump magnetic field amplitude $B_o(z)$ builds up adiabatically and reaches a constant value inside the interaction region. We assume that the electron beam is generated far to the left of the interaction region, where the pump field vanishes. In general the beam will be produced with a thermal momentum spread in the transverse as well as the longitudinal direction. However, the transverse momentum spread, $P_{\perp th}$, may be neglected if it is much less than the ordered transverse momentum $|e|B_o/ck_o$, induced by the pump field. Unless the pump amplitude is unusually small, the condition, $P_{\perp th} << |e|B_o/ck_o$ can be easily satisfied. Then the transverse momentum is proportional only to the pump amplitude and the solutions of the equations of motion are accurately given by $\alpha = \beta = 0$ in Eqs. (4). Thus, for $P_{\perp th} << |e|B_o/ck_o$, we may choose the equilibrium distribution function to be of the form

$$g^{(0)}(\alpha,\ \beta,\ u) = n_o\delta(\alpha)\ \delta(\beta)\ g_o(u), \tag{23}$$

where n_o is the ambient beam density far to the left of the interaction region. The normalization of $g_o(u)$ is such that

$$\int_o^\infty du \, \frac{u}{u_z(u)} \, g_o(u) = 1,$$

where $u_z(u) = p_z(\alpha = 0, \beta = 0, u, z) = (u^2 - |e|^2 B_o^2/c^2 k_o^2)^{1/2}$. We may remark that for $\alpha = \beta = 0$, each particle has constant axial momentum. This is a rather important property of the pump field in Eq. (1). Since the equilibrium axial momentum and velocity do not oscillate as a function of z the pump field does not introduce an effective longitudinal spread in velocity which would limit the effectiveness of the scattering process. The appropriate functional form of $g_o(u)$ will depend on the scattering process being considered; we shall leave it general for the moment. Using the distribution in Eq. (23) it is straightforward to evaluate the Fourier amplitudes of the driving current density in Eq. (20). The details of this calculation are given in Appendix 1. Defining

$$\Psi_\pm(z) \equiv \left(\frac{\omega}{v_z} \pm k_o\right) z,$$

we find

$$\tilde{J}_\pm(z) = \frac{-\omega_b^2}{4\pi} \int_0^\infty \left[\frac{u}{\gamma u_z c} \left\{ \left(1 + \frac{\beta_\perp^2}{2}\right) \left[\tilde{A}_\pm(z) - \tilde{A}_\pm(0)\, e^{i\omega z/v_z}\right] \right.\right.$$

$$+ \frac{\beta_\perp^2}{2} \frac{\omega}{k_o v_z} e^{i\Psi_\mp(z)} \left[\tilde{A}_+(0)\left(1 - e^{ik_o z}\right) - \tilde{A}_-(0)\left(1 - e^{-ik_o z}\right)\right]$$

$$\left.\left. + \frac{\beta_\perp^2}{2} e^{i\Psi_\mp(z)} \left[\tilde{A}_\mp(z) e^{-i\Psi_\pm(z)} - \tilde{A}_\mp(0) e^{\mp ik_o z}\right] \right\} \right.$$

$$\left. + \frac{m_o \beta_\perp}{2} e^{i\Psi_\mp(z)} \int_0^z \left\{ \frac{\partial \tilde{\phi}(z')}{\partial z'} e^{-i\omega z'/v_z} + i\frac{\omega \beta_\perp}{c} \left[\tilde{A}_+(z') e^{-i\Psi_-(z')} + \tilde{A}_-(z') e^{-i\Psi_+(z')}\right] \right\} dz' \, \frac{\partial}{\partial u} \right] g_o \, du$$

(24a,b)

$$\tilde{J}_z(z) = -\frac{\omega_b^2}{8\pi} e^{i\omega z/v_z} \int_0^\infty \left[\frac{u}{\gamma u_z c} \frac{\omega}{k_o v_z} \beta_\perp \left[\tilde{A}_+(0)\left(e^{ik_o z} - 1\right) - \tilde{A}_-(0)\left(e^{-ik_o z} - 1\right)\right] \right.$$

$$\left. - m_o \int_0^z \left\{ \frac{\partial \tilde{\phi}(z')}{\partial z'} + \frac{i\omega\beta_\perp}{c} \left[\tilde{A}_+(z') e^{ik_o z'} + \tilde{A}_-(z') e^{-ik_o z'}\right] \right\} e^{-i\omega z'/v_z} \, dz' \frac{\partial}{\partial u} \right] g_o(u) \, du, \quad (24c)$$

where $\omega_b = (4\pi|e|^2 n_o/m_o)^{1/2}$ is the beam plasma frequency, $\beta_\perp = \Omega_o/\gamma k_o v_z$ is the transverse beam velocity normalized to v_z, $\Omega_o = |e|\, B_o/m_o c$, and $v_z = u_z/\gamma m_o$.

It is informative to consider at this point the current density $\mathbf{J}(z, t)$ in the absence of the pump field in order to find the pump-free eigenmodes of the system. Setting $B_o = 0$ we find from Eqs. (24) that

$$\tilde{J}_\pm(z)\Big|_{B_o=0} = -\frac{\omega_b^2}{4\pi c}\int_o^\infty \frac{1}{\gamma}\left[\tilde{A}_\pm(z) - \tilde{A}_\pm(0)\, e^{i\frac{\omega}{v_z}z}\right] g_o\, du,$$

$$\tilde{J}_z(z)\Big|_{B_o=0} = +\frac{\omega_b^2}{8\pi} m_o \int_o^\infty \int_o^z \frac{\partial\tilde{\phi}(z')}{\partial z'}\, e^{-i\frac{\omega}{v_z}(z'-z)}\, dz'\, \frac{\partial}{\partial u} g_o\, du, \tag{25}$$

where $v_z\Big|_{B_o=0} = u/\gamma m_o$. For the moment we will consider the eigenmodes for $z >> 0$. In this case we can take $\tilde{A}_\pm(z)$ and $\tilde{\phi}(z)$ to be plane waves of the form $\tilde{A}_\pm(z) = \tilde{A}_\pm(0)\exp(i k_\pm z)$ and $\tilde{\phi}(z) = \tilde{\phi}(0)\exp(i k z)$ where $k_\pm$ and k are real constants. Neglecting the free streaming terms in Eqs. (24), *i.e.*, $\exp\left[i\frac{\omega}{v_z}z\right]$, because they eventually phase mix away, we obtain for $z >> 0$

$$\tilde{J}_\pm(z) = -\frac{\omega_b^2}{4\pi c}\int_o^\infty \frac{g_o\, du}{\gamma}\,\tilde{A}_\pm(z),$$

$$\tilde{J}_z(z) = \frac{-\omega_b^2}{8\pi} m_o \omega \int_o^\infty \frac{\partial g_o/\partial u\, du}{\omega - v_z k}\,\tilde{\phi}(z). \tag{26}$$

Combining the current densities given by Eqs. (19) and (26) with the wave equations in (21), we arrive at the conventional dispersion relations for the transverse electromagnetic field and the electrostatic field:

$$D(\omega, k_\pm)\,\tilde{A}_\pm(z) = 0;$$

$$(1 + \chi(\omega, k))\,\tilde{\phi}(z) = 0; \tag{27}$$

where χ is the electron susceptibility

$$\chi(\omega, k) = \frac{\omega_b^2}{k}\int \frac{m_o\, \partial g_o/\partial u\, du}{\omega - v_z k} \tag{28a}$$

and

$$D(\omega,\ k_{\pm}) = \omega^2 - c^2k_{\pm}^2 - \omega_b^2 \int_o^{\infty} g_o/\gamma\ du. \tag{28b}$$

It is now possible to show that for the doppler-upshifted backscattered wave we can consider the A_+ or A_- wave separately. In the presence of the pump field it will be shown that the products $D(\omega,k_{\pm})\ \tilde{A}_{\pm}(z)$ are no longer zero, but are equal to a small coupling term proportional to B_o^2. In order for $\tilde{A}_+(z)$ to be excited it is necessary for $D(\omega,\ k_+) \approx 0$; likewise, for $\tilde{A}_-(z)$ to be excited $D(\omega,k_-)$ must be very small. It can be shown by carefully scrutinizing Eqs. (24) that k_+ and k_- are connected by the relationship $k_+ = k_- - 2k_o$. Because of this relationship, the functions $D(\omega,\ k_+)$ and $D(\omega,\ k_-)$ cannot be simultaneously zero for the same backscattered upshifted frequency. Therefore, A_+ and A_- are independently excited. Furthermore, by simply changing the sign of ω and either k_+ or k_- we see that the behavior of the two waves are identical. Hence, in the remainder of this paper we shall arbitrarily take the wave at $(\omega,\ k_+)$ to be resonant, *i.e.*, $D(\omega,\ k_+) \approx 0$, and the $(\omega,\ k_-)$ wave to be nonresonant, *i.e.*, $D(\omega,\ k_-) \neq 0$. This amounts to keeping only the $\tilde{A}_+$ wave and neglecting the $\tilde{A}_-$ wave. We will now evaluate the growth rates and saturation level for various scattering regimes.

III. GAIN AND SATURATION LEVEL IN VARIOUS FEL REGIMES

Case 1. Low Gain, Tenuous-Cold-Beam Limit

As our first example we will consider the low gain, (*i.e.*, "short cavity") scattering process in which collective effects are unimportant. This limit corresponds to the parameter regime of the recent experiments carried out at Stanford University with highly relativistic ($\leqslant$ 48 MeV), low-current ($\leqslant$ 2.4A) electron beams. Collective effects are manifested by the space charge potential ϕ, which arises from the charge bunching under the action of the pondermotive potential ϕ_{pond}. In the very tenuous beam limit the scalar potential is much less than the pondermotive potential. It can be shown that collective effects can be neglected when the magnitude of the electron susceptibility χ is small compared to unity. In this limit we can set $\phi = 0$ and represent the scattered electromagnetic wave in the form (see Eq. (11))

$$\tilde{A}_+(z) = \tilde{A}_+(0)\, e^{i\int_o^z k_+(z')\,dz'} \tag{29}$$

where $k_+(z) \equiv k_{o+} + \delta k(z)$, $k_{o+} >> |\delta k|$ is real and constant and δk is complex and a slowly varying function of z. Using this form for the field we find from Eq. (24a),

$$\tilde{J}_+(z) = -\frac{\omega_b^2}{4\pi c}\int_o^\infty \left[\frac{u}{\gamma u_z}\left\{\left(1+\frac{\beta_\perp^2}{2}\right)\left\{1-e^{-i\psi(u,\,z)}\right\} - \frac{\beta_\perp^2}{2}\,\frac{\omega}{k_o\, v_z}\, e^{-i\psi(u,\,z)}\,(1-e^{-ik_o z})\right\}\right.$$
$$\left. + i\frac{\beta_\perp^2}{2}\,\omega m_o e^{-i(\psi(u,\,z)+k_o z)}\int_o^z dz'\, e^{i(\psi(u,\,z')+k_o z')}\,\frac{\partial}{\partial u}\right] g_o\,\tilde{A}_+(0)\, e^{i\int_o^z k_+(z')\,dz'}\,du, \tag{30}$$

where $\psi(u,\,z) = \int_o^z k_+(z')\,dz' - \omega z/v_z$. In the context of Eqs. (29) and (30) the wave equation (21b) can be used to derive the following dispersion relation:

$$k_{o+}^2 - \frac{\omega^2}{c^2} + 2k_{o+}\delta k(z) = -\frac{\omega_b^2}{c^2}\,\mu(\omega,\, k_{o+},\, z), \tag{31}$$

where

$$\mu(\omega,\, k_{o+},\, z) = \int_o^\infty \left[\frac{u}{\gamma u_z}\left\{\left(1+\frac{\beta_\perp^2}{2}\right)\left(1-e^{-i\left((k_{o+}-\frac{\omega}{v_z}\right)z}\right)\right.\right.$$
$$\left.\left. - \frac{1}{2}\,\beta_\perp^2\,\frac{\omega}{v_z k_o}\, e^{-i\left(k_{o+}-\frac{\omega}{v_z}\right)z}\,(1-e^{-ik_o z})\right\}\right.$$

$$- \frac{1}{2}\,\beta_\perp^2\, m_o v_z \omega\, \frac{(1 - e^{-i(k - \frac{\omega}{v_z})z})}{\omega - v_z k}\, \frac{\partial}{\partial u}\Bigg] g_o\, du \tag{32}$$

and where $k = k_{o+} + k_o$.

Note that in obtaining (31) we used the facts that in the present scattering limit, $|\delta k(z)| << k_{o+}$, $\int_0^z \delta k(z')dz' << 1$ and $\delta k(z)$ is a very "weak" function of z, so that $\psi(u, z)$ has been approximated in the RHS of Eq. (32) by $(k_{o+} - \omega/v_z)z$. Solving for the imaginary part of Eq. (31), we find

$$\begin{aligned} \mathrm{Im}(\delta k) = \frac{-\omega_b^2/c^2}{2k_{o+}} \int_0^\infty \Bigg[& \frac{1}{2}\,\beta_\perp^2 m_o \omega\, \frac{\sin(\omega/v_z - k)z}{(\omega/v_z - k)}\, \frac{\partial}{\partial u} \\ & - \frac{u}{\gamma u_z} \Bigg\{ (1 + \beta_\perp^2/2)\sin(\omega/v_z - k_{o+})z \\ & + \frac{\beta_\perp^2}{2}\, \frac{\omega}{v_z k_o} \left[\sin(\omega/v_z - k_{o+})z - \sin(\omega/v_z - k)z \right] \Bigg\} \Bigg] g_o du. \end{aligned} \tag{33}$$

The total gain in amplitude of the scattered wave, over the interaction length L, is given by

$$\begin{aligned} G_L &= - \int_0^L Im(\delta k(z'))\, dz' \\ &= \frac{\omega_b^2/c^2}{2k_{o+}} \int_0^\infty \Bigg[\frac{\beta_\perp^2}{4}\, m_o \omega L^2 \left[\frac{\sin(k - \omega/v_z)\, L/2}{(k - \omega/v_z) L/2} \right]^2 \frac{\partial}{\partial u} \\ &\quad - \frac{u}{\gamma u_z} \Bigg\{ \frac{\beta_\perp^2}{2}\, \frac{\omega}{v_z k_o}\, L\, \frac{\sin^2(k - \omega/v_z) L/2}{(k - \omega/v_z) L/2} \\ &\quad - \left[1 + \frac{\beta_\perp^2}{2}\, \frac{\omega}{v_z k_o} \right] L\, \frac{\sin^2(k_{o+} - \omega/v_z) L/2}{(k_{0+} - \omega/v_z) L/2} \Bigg\} \Bigg] g_o\, du. \end{aligned} \tag{34}$$

Equation (34) is a complicated expression for G_L which depends on $g_o(u)$. If, however, g_o is such that the phase of the sine functions in Eq. (34) does not vary appreciably over the range of v_z for which g_o is non-zero, then to evaluate the integral we may take

$$g_o(u) = \frac{u_z}{u}\, \delta(u - u_o). \tag{35}$$

The condition for the applicability of (35) is that the axial thermal velocity spread V_{th} of the beam satisfy

$$V_{th} << \frac{\pi c}{\gamma_{zo}^2 k_o L} = \frac{\lambda_s c}{L}. \tag{36}$$

The thermal energy spread E_{th} of the beam in general is given by

$$E_{th} = \gamma_o \gamma_{zo}^2 m_o v_{zo} V_{th}, \tag{37}$$

and for a highly relativistic beam, inequality (36) may be rewritten as

$$\frac{E_{th}}{E_o} << \gamma_{zo}^2 \frac{\lambda_s}{L}, \tag{38}$$

where $E_o = (\gamma_o - 1) m_o c^2 \simeq \gamma_o m_o c^2$ is the kinetic energy of the particles. In the experiments to date this condition is satisfied by roughly one order of magnitude.

For a highly relativistic beam, we may approximate $v_z \simeq c$, $u_z \simeq u$, $k_{o+} \simeq 2\gamma_z^2 k_o$. Then using Eq. (35), the total gain becomes.

$$\begin{aligned} G_L &= \left(\frac{\xi}{2\gamma_{zo}}\right)^2 k_o L \left[\frac{\beta_{o\perp}^2 \gamma_{zo}^2}{2} \left\{(k_o L)^2 \frac{\partial}{\partial \theta_o}\left(\frac{\sin\theta_o}{\theta_o}\right)^2 + 2\frac{\sin^2\theta_o}{\theta_o}\right\}\right. \\ &\qquad \left. - (1 + \beta_{o\perp}^2 \gamma_{zo}^2) \frac{\sin^2(\theta_o + k_o L/2)}{(\theta_o + k_o L/2)}\right] \\ &\equiv \left(\frac{\xi}{2\gamma_{zo}}\right)^2 k_o L \; F(\theta_o,\; k_o L,\; \beta_{o\perp}\gamma_{zo}), \end{aligned} \tag{39}$$

where $\xi = \omega_b/(\sqrt{\gamma_o} c k_o)$ is the beam strength parameter, $\gamma_o = \gamma(u_o)$, $\gamma_{zo} = \gamma_z(u_o)$, $\beta_{0\perp} = \beta_\perp(u_o)$, and $\theta_o = (\omega/v_{zo} - k_{o+} - k_o) L/2$. In deriving Eq. (39) we have used the fact that

$$\frac{\partial}{\partial u} = -\frac{\omega}{v_z^2} \frac{L}{2} \frac{u}{m_o \gamma u_z \gamma_z^2} \frac{\partial}{\partial \theta_o}.$$

In Figures (2a,b) we exhibit the function $F(\theta_o,\; k_o L,\; \beta_{0\perp}\gamma_{zo})$ for the cases where $L = 160l$ and $L = l$. If the interaction region consists of a large number of pump periods, $k_o L >> 1$, the first term of the gain expression in Eq. (39) is dominant. For this case

$$G_L \approx \frac{\xi^2}{8} \beta_{o\perp}^2 (k_o L)^3 \frac{\partial}{\partial \theta_o}\left(\frac{\sin\theta_o}{\theta_o}\right)^2. \tag{40}$$

The function $\partial/\partial\theta_o (\sin\theta_o/\theta_o)^2$ has a maximum value of 0.54 when $\theta_o = -1.3$, therefore, the maximum value of gain is

$$G_{L_{max}} \approx (\xi/4)^2 \beta_{o\perp}^2 (k_o L)^3. \tag{41}$$

These expressions for the gain are similar to results found previously by Motz (1951), Sukhatme and Wolff (1973), Colson (1976), Hopf *et al.* (1976a), and Kroll and McMullin (1978).

A detailed calculation of the efficiency in the free-election-laser low-gain regime was presented by Hopf *et al.*, who found that the efficiency was approximately given by

$$\eta = (\lambda_s/L)\,\gamma^2 \tag{42}$$

where $\lambda_s = 2\pi/k_+$. It is possible to obtain this result from general arguments based on electron trapping in the longitudinal wave associated with the electron beam. (The total longitudinal wave in general consists of both the space charge potential and ponderomotive potential waves.) The following discussion, which will be used to estimate saturation efficiencies as well as the saturated electromagnetic field amplitude, may be applied to all the cases involving scattering from a cold beam in which trapping saturates the process.

For maximum spatial gain, the phase velocity $v_{ph} = \omega/Re(k)$ of the longitudinal wave and the directed axial beam velocity v_{zo} are related, in the linear development of the instability, by an expression of the form

$$v_{ph} - v_{zo} = -\Delta v \tag{43}$$

where $\Delta v > 0$ is a small term which depends on the particular scattering regime being considered. In the low-gain, tenuous-beam limit we have just discussed, for example, the gain G_L maximizes at $\theta_o = -1.3$; this condition may be written in the form (43). In the high-gain regimes to be discussed later, in which the scattering process may be described by a dispersion relation homogeneous in space, a condition of the form (43) will be seen to describe the condition of maximum coupling between the beam and the backscattered wave. Since wave growth will occur for $\Delta v > 0$, we can interpret this condition as stating that the phase velocity of the longitudinal wave must be less than the axial beam velocity in order for beam kinetic energy to be converted into wave energy. The wave amplitude increases, at the expense of the beam

kinetic energy, until the beam electrons become trapped at the bottoms of the potential wells of the longitudinal wave. At this point the wave reaches its maximum amplitude and the average beam kinetic energy reaches a minimum. The average axial beam speed at saturation, $v_{z,s}$, is approximately given by the trapping condition

$$v_{ph} - v_{z,s} = + \Delta v \tag{44}$$

Therefore, at saturation the kinetic energy lost by the beam corresponds to a decrease in axial beam speed of $v_{zo} - v_{z,s} = 2\Delta v$. It should be noted that when the beam electrons are trapped at the bottom of the potential wells of the wave they are modulated spatially but are fairly monoenergetic. The decrease in beam energy can be equated to the increase in wave energy. In this way the efficiency and saturated field amplitude of the scattering process can be estimated.

In the case of a relativistic electron beam the change in kinetic energy at saturation, when the beam particles are deeply trapped, is

$$\Delta E_{K.E.} = (\gamma(v_{zo}) - \gamma(v_{z,s}))\ m_o c^2$$

$$\simeq 2 \frac{\partial \gamma(v_z = v_{zo})}{\partial v_z} \Delta v\ m_o c^2 = 2\gamma_o \gamma_{zo}^2\ m_o v_{zo} \Delta v. \tag{45}$$

The efficiency is then given by

$$\eta = \frac{\Delta E_{K.E.}}{(\gamma_o - 1)\ m_o c^2} \simeq 2\gamma_{zo}^2\ \Delta v/c \tag{46}$$

where the last expression in (46) is for a highly relativistic beam, $v_{zo} \simeq c$. The amplitude of the scattered electromagnetic fields at saturation can now be obtained by the following argument.

In the steady state, conservation of total energy flux states that

$$\frac{\partial}{\partial z}\left[nv_z(\gamma - 1)\ m_o c^2 \hat{e}_z + \frac{c}{4\pi}\ \mathbf{E} \times \mathbf{B}\right] = 0.$$

Integrating from the input of the interaction region, $z = 0$, to the point where the scattered

field is maximum, $z = z_{sat}$, gives

$$|\tilde{A}_+(z = z_{sat})|^2 \approx |\tilde{A}_+(z = 0)|^2 + \frac{4\pi n_o c^2}{\omega^2} \Delta E_{K.E.}$$

$$\approx |\tilde{A}_+(z = 0)|^2 + \frac{4\pi n_o}{(\omega/c)^2} \eta \gamma_o m_o c^2. \tag{47}$$

In obtaining $|\tilde{A}_+(z = z_{sat})|$ we used the fact that the fields were given by Eqs. (11), $\tilde{A}_- = 0$, $\mathbf{E} \times \mathbf{B} \approx (\omega^2/c^2)\ |\tilde{A}_+(z)|^2$ and $v_{zo} = v_{z,s} \approx c$. The magnitude of the transverse electric field at saturation becomes

$$|\mathbf{E}|_{\text{sat}} = \frac{\omega}{c}\ |\tilde{A}_+(z = z_{sat})|. \tag{48}$$

The results for the efficiency and saturated transverse electric field in Eqs. (46) and (48) apply to those scattering processes in which electron trapping is responsible for saturation. To apply these results to the low gain scattering process in Case 1, we note that the condition for maximum gain over a distance $z_{sat} = L$ is given by $\theta_o = -1.3$, which when put in the form of Eq. (43) becomes

$$v_{ph} - v_{zo} = \frac{-2.6}{kL}\ v_{zo} = -\Delta v. \tag{49}$$

Substituting Eq. (49) into Eq. (46) the estimated value of efficiency is

$$\eta \approx 5.2\ \gamma_{zo}^2/(kL) \approx \gamma_{zo}^2\ \lambda_s/L, \tag{50}$$

in agreement with Eq. (42), where $\lambda_s = 2\pi/k_{o+} \approx 2\pi/k$ is the wavelength of the scattered wave. The assumption implicit in the above argument is that the length L and the energy lost by the electrons are matched so that the trapping occurs at the end of the system. The energy lost by the electrons, however, goes into the scattered wave and depends upon the amplitude of the input signal. To find the field amplitude necessary to effectuate this energy change in the length L we note that in the low gain limit $G_L \ll 1$, we have $|\tilde{A}_+(z = z_{sat} = L)|$ $\approx |\tilde{A}_+(z = 0)|\ (1 + G_L)$ and thus Eq. (48) gives

$$|\tilde{A}_+(z = 0)|^2 = \frac{2\pi n_o}{(\omega/c)^2} \left[\frac{\eta}{G_L}\right] \gamma_o m_o c^2.$$

At maximum gain conditions we have, using Eq. (41),

$$|\tilde{A}_+(z=0)| = \sqrt{5.2}\left(\frac{\gamma_o}{\gamma_{zo}^2}\right)\left(\frac{m_o c^2}{|e|}\right)\frac{1}{\beta_{o\perp}}\,\frac{1}{(k_o L)^2}\,. \tag{51}$$

Since $|\tilde{A}_+(z=z_{sat})| \approx |\tilde{A}_+(z=o)|$, the saturated transverse electric field amplitude can be estimated from Eqs. (48) and (51) as

$$|\mathbf{E}|_{sat} \approx 2\sqrt{5.2}\left(\frac{m_o c^2}{|e|}\right) k_o\,\frac{\gamma_o}{\beta_{o\perp}(k_o L)^2}\,. \tag{52}$$

Equation (52) gives the required input signal necessary to achieve the efficiency in Eq. (46) at maximum gain conditions. This input signal level is required for optimum efficiency. If the input signal is weaker than this value, saturation of the wave will not occur within the length L. If it is stronger, saturation will occur before the beam reaches the end of the interaction region, resulting in smaller total gain.

Case 2. High Gain, Tenuous-Thermal-Beam Limit

We now consider the high gain limit with a tenuous thermal beam; this limit is the relativistic analog of stimulated Compton scattering. We again neglect the space charge potential but now assume that the wave e-folds many times, hence $|\tilde{A}(z)| >> |\tilde{A}(0)|$ except near $z = 0$. Since for this case $-Im\int_o^z k_+(z')\,dz' >> 1$, the driving current is found from (30) to take the form

$$\tilde{J}_+(z) = -\frac{\omega_b^2}{4\pi c}\int_o^\infty \left[\frac{u}{\gamma u_z}\left(1+\frac{\beta_\perp^2}{2}\right) - \frac{\beta_\perp^2}{2}\,\omega\, v_z . m_o \frac{\partial/\partial u}{\omega - v_z k}\right] g_o\, du\, \tilde{A}_+(0)\, e^{ik_+ z} \tag{53}$$

where k_+ is complex and independent of z. Substituting Eq. (53) into Eq. (21b) gives the dispersion relation

$$k_+^2 - \omega^2/c^2 = -\omega_b^2/c^2 \int_o^\infty \left[\frac{u}{\gamma u_z}\left(1+\frac{\beta_\perp^2}{2}\right) g_o(u) - \frac{\beta_\perp^2}{2}\,\omega\, v_z\, m_o\,\frac{\partial g_o/\partial u}{\omega - v_z k}\right] du, \tag{54}$$

where $k = k_+ + k_o \equiv k_r + ik_i$. In the Compton scattering regime the phase velocity of the ponderomotive wave is resonant with a small fraction of the thermal beam electrons (see Fig. 3). We now consider the case where the thermal width of the particle distribution function is

large compared to the width of the wave distribution $(\omega - v_z k)^{-1}$. If the thermal velocity spread of the relativistic beam is such that

$$V_{th} >> |c\ k_i/k_r|, \tag{55}$$

then the pump wave scatters from single particles. When the inequality (55) is satisfied we can take the imaginary parts of both sides of Eq. (54) and use the fact that

$$Im\left(\frac{1}{\omega - v_z k}\right) = -\frac{\pi}{|k_r|}\ \delta(v_z - \omega/k_r)$$

as k_i approaches zero from negative values. Because $v_z = c(u^2 - u_{0\perp}^2)^{1/2}/(u^2 + m_o^2 c^2)^{1/2}$, we can write

$$\delta(v_z - \omega/k_r) = \frac{\gamma \gamma_z^2 m_o u_z}{u}\ \delta(u - u_{ph}) \tag{56}$$

where $\partial v_z/\partial u = u/(\gamma\ \gamma_z^2 m_o u_z)$, $u > 0$, $u_{ph} \equiv \gamma_{ph}(\beta_{ph}^2\ m_o^2\ c^2 + u_{0\perp}^2)^{1/2}$, $u_z = (u^2 - u_{o\perp}^2)^{1/2}$, $\beta_{ph} \equiv \omega/k_r c$, $\gamma_{ph} \equiv (1 - \beta_{ph}^2)^{-1/2}$, and $u_{0\perp}^2 = (|e|\ B_o/ck_o)^2$. The imaginary part of k, from Eq. (54) using Eq. (56), is given by

$$k_i = \frac{-\omega_b^2}{4k_r c^2}\ \frac{\pi}{|k_r|}\ \beta_\perp^2\ v_z\ m_o\ \omega\ \frac{\gamma\ \gamma_z^2\ m_o\ u_z}{u}\ \frac{\partial g_o}{\partial u}\bigg|_{u=u_{ph}}. \tag{57}$$

For a drifting electron beam with average total momentum u_o, we can take $g_o(u)$ to be Maxwellian-like of the form

$$g_o(u) = \frac{u_z/u}{\sqrt{2\pi}\,U_{th}}\ e^{-(u-u_o)^2/(2U_{th}^2)}, \tag{58}$$

such that $\int_o^\infty du\ g_o\ u/u_z = 1$. Substituting (58) into (57) we get for a highly relativistic beam the result

$$k_i = \frac{\omega_b^2}{8k_o}\ \sqrt{\pi}\ \beta_\perp^2\ \frac{\gamma\ m_o^2}{U_{th}^2}\ x\ e^{-x^2}\bigg|_{u=u_{ph}} \tag{59}$$

where $x = (u - u_o)/(\sqrt{2}\ U_{th})$. The function xe^{-x^2} has a minimum value of -0.43 when $x = -1/\sqrt{2}$, *i.e.*, $u_{ph} = u_o - U_{th}$ Since for a highly relativistic beam the thermal energy spread E_{th} is very nearly equal to cU_{th}, the maximum spatial growth rate becomes

$$|k_i|_{max} \approx \frac{\sqrt{\pi}}{20}\ \xi^2 k_o\ \beta_{o\perp}^2 \left(\frac{E_o}{E_{th}}\right)^2. \tag{60}$$

where, as before, $E_o \approx \gamma_o mc^2$, and $\xi = \omega_b/(\sqrt{\gamma_o}\ ck_o)$.

These results for the growth rate agree with those of Lin and Dawson (1975), Hasegawa *et al.* (1976), Kroll and McMullin (1978), and Sprangle and Drobot (1978).

In order to estimate the efficiency in this stimulated Compton regime, we first note that only a small fraction of the beam particles are resonant with the unstable wave. This fraction is determined by the width of the spectrum of the spatially growing wave. The width of the wave spectrum in velocity space is given to a good approximation by

$$\delta v_w \approx |2ck_i/k| << V_{th}. \tag{61}$$

In momentum space (see Fig. 4) this width becomes

$$\delta u_w \approx \frac{\partial u}{\partial v_z}\bigg|_{v_z=v_{zo}} \delta v_w \approx |2\gamma_o \gamma_{zo}^2 m_o c k_i/k|$$

$$\approx |\gamma_o m_o c k_i/k_o| << U_{th} \tag{62}$$

As the backscattered electromagnetic wave grows, a small fraction of the beam particles, those with momenta between $u_{ph} - \delta u_w/2$ and $u_{ph} + \delta u_w/2$, become trapped in the potential associated with the ponderomotive wave. As this happens, the distribution function begins to flatten out near $u = u_{ph}$ and $\partial g/\partial u$ decreases until it vanishes. A plateau is then formed and the distribution becomes stable with respect to the initially unstable wave because $\partial g/\partial u\big|_{u=u_{ph}} = 0$ (see Fig. 4). The change in kinetic energy between the initial and final distribution functions is given by

$$\delta E_{K.E.} = \frac{n_o m_o c^2}{\sqrt{2\pi}\, U_{th}} \int_{u_{ph}-\delta u_w/2}^{u_{ph}+\delta u_w/2} (\gamma - 1) \left[e^{-(u-u_o)^2/2U_{th}^2} - e^{-1/2} \right] du, \tag{63}$$

where we have used the fact that $u_{ph} = u_o - U_{th}$ for the maximum growth rate. Since $\delta u_w << U_{th}$, evaluation of Eq. (63) gives

$$\delta E_{K.E.} \approx \frac{n_o}{\sqrt{2\pi}} e^{-1/2} \left(\frac{\delta u_w}{2U_{th}} \right)^2 \left(\frac{\partial \gamma}{\partial u} \right)_{u=u_{ph}} \delta u_w\, m_o c^2$$

$$\approx \frac{n_o c}{4\sqrt{2\pi}} \left(\frac{\delta u_w}{U_{th}} \right)^3 U_{th}, \tag{64}$$

where $\delta u_w/U_{th}$ is evaluated from Eq. (62) with k_i given by Eq. (60) and is given by

$$\delta u_w / U_{th} = \frac{\sqrt{\pi}}{20}\, \xi^2\, \beta_{o\perp}^2 (E_o/E_{th})^3 << 1. \tag{65}$$

The efficiency using Eq. (64) is given by

$$\eta = \frac{\delta E_{K.E.}}{n_o(\gamma_o - 1)\, m_o c^2} = \frac{1}{4\sqrt{2\pi}} \left(\frac{\delta u_w}{U_{th}}\right)^3 \frac{E_{th}}{E_o}. \tag{66}$$

Using the expression for the efficiency in (66) and Eq. (47) together with (48), we find that the electric field amplitude at saturation is

$$|\mathbf{E}|_{\text{sat}} = \frac{m_o c^2}{|e|}\, \gamma_o\, \xi\, k_o \left\{\left(\frac{\delta u_w}{U_{th}}\right)^3 \frac{E_{th}/E_o}{4\sqrt{2\pi}}\right\}^{1/2} \tag{67}$$

The requirement on the beam thermal velocity is stated in Eq. (55). In terms of the ratio E_{th}/E_o, this condition becomes

$$E_{th}/E_o >> \left(\frac{\sqrt{\pi}}{40}\, \xi^2\, \beta_{o\perp}^2\right)^{1/3}, \tag{68}$$

where Eqs. (55), (60) and (37) have been used.

Case 3. High Gain, Dense-Cold-Beam Limit

In this limit, we shall retain the space charge scalar potential ϕ which arises from charge bunching by the ponderomotive potential. Because the scattered fields are assumed to e-fold many times within the interaction region we may neglect boundary terms at $z = 0$ and choose $\tilde{\phi}$ and $\tilde{A}_+$ to have the form (see Eq. (11))

$$\begin{aligned} \tilde{\phi}(z) &= \tilde{\phi}(0) e^{ikz}, \\ \tilde{A}_+(z) &= \tilde{A}_+(0) e^{ik_+ z}, \end{aligned} \tag{69}$$

where k_+ and k are complex constants.

Substituting the fields in (69) into Eqs (24) and taking the high gain limit, *i.e.*, $|\exp(i\,k\,z)| >> 1$ and $|\exp(i\,k_+ z)| >> 1$, the driving current densities become

$$\begin{aligned} \tilde{J}_+(z) = -\frac{\omega_b^2}{8\pi} \int_o^\infty \Bigg[&\left\{ \frac{u}{\gamma u_z c}\,(2 + \beta_\perp^2) - \frac{\beta_\perp^2 m_o \nu_z \omega / c}{\omega - \nu_z (k_+ + k_o)}\, \frac{\partial}{\partial u} \right\} \tilde{A}_+(0)\, e^{ik_+ z} \\ &- \frac{\beta_\perp m_o \nu_z k\, \partial/\partial u}{\omega - \nu_z k}\, \tilde{\phi}(0)\, e^{i(k - k_o)z} \Bigg] g_o\, du, \end{aligned} \tag{70a}$$

$$\tilde{J}_z(z) = -\frac{\omega_b^2}{8\pi}\int_o^\infty m_o\left[\frac{\nu_z k}{\omega - \nu_z k}\,\tilde{\phi}(0)\,e^{ikz} + \frac{\beta_\perp \nu_z \omega/c}{\omega - \nu_z(k_+ + k_o)}\,\tilde{A}_+(0)\,e^{i(k_+ + k_o)z}\right]\frac{\partial g_o}{\partial u}\,du. \tag{70b}$$

We see immediately from Eqs. (70) that the selection rule between the wavenumbers of the three waves is

$$k = k_+ + k_o. \tag{71}$$

The coefficients of the driving currents $\tilde{J}_+$ and $\tilde{J}_z$, using Eq. (70), can be written in the form

$$\tilde{J}_+(z) = -\frac{\omega_b^2}{8\pi c}\left[\left\{2\left\langle\frac{u}{\gamma u_z}\right\rangle + \left(\frac{\Omega_o}{ck_o}\right)^2 S(\omega,k)\right\}\tilde{A}_+(0) - \frac{\Omega_o}{ck_o}\,\frac{c^2k^2}{\omega_b^2}\,\chi_\gamma(\omega,k)\tilde{\phi}(0)\right]e^{ik_+z},$$

$$\tilde{J}_z(z) = -\frac{\omega k}{8\pi}\left[\chi(\omega,k)\tilde{\phi}(0) + \frac{\Omega_o}{ck_o}\,\chi_\gamma(\omega,k)\,\tilde{A}_+(0)\right]e^{ikz}, \tag{72}$$

where

$$\langle(\cdots)\rangle = \int_0^\infty du\, g_o(u)(\cdots),$$

$$S(\omega,k) = \left\langle\frac{uc^2}{\gamma^3 u_z \nu_z^2}\right\rangle - \omega c\int_0^\infty \frac{m_o c\,\partial g_o/\partial u}{\gamma^2 v_z(\omega - \nu_z k)}\,du,$$

$$\chi(\omega,k) = \frac{\omega_b^2}{k}\int_0^\infty \frac{m_o\,\partial g_o/\partial u}{\omega - \nu_z k}\,du,$$

$$\chi_\gamma(\omega,k) = \frac{\omega_b^2}{k}\int_0^\infty \frac{m_o\,\partial g_o/\partial u}{\gamma(\omega - \nu_z k)}\,du.$$

Substituting Eqs. (69) into the wave equations shown in (21) gives

$$\tilde{\phi}(0)\,e^{ikz} = \frac{-\Omega_o}{ck_o}\,\frac{\chi_\gamma(\omega,k)}{1+\chi(\omega,k)}\,\tilde{A}_+(0)\,e^{ikz},$$

$$\left[D(\omega,k_+) - \frac{\omega_b^2}{2}\left(\frac{\Omega_o}{ck_o}\right)^2 S(\omega,k)\right]\tilde{A}_+(0)\,e^{ik_+z} = -\frac{c^2k^2}{2}\,\frac{\Omega_o}{ck_o}\,\chi_\gamma(\omega,k)\,\tilde{\phi}(0)\,e^{ik_+z} \tag{73}$$

The first of the equations in (73) can be put into an illuminating form by noting that to a good approximation γ can be taken out of the integral in the definition of $\chi_\gamma(\omega, k)$, since it is a slowly varying function of u. With this approximation together with the definition of the

ponderomotive potential in Eq (22) we find that

$$\tilde{\phi}(z) = \frac{\chi(\omega, k)/2}{1 + \chi(\omega, k)} \tilde{\phi}_{pond}(z), \tag{74}$$

where $\tilde{\phi}(z) = \tilde{\phi}(0) \exp(ikz)$. In Eq. (74) we see explicitly the fact that the ponderomotive potential drives the space charge potential.

Combining the two equations in (73) we arrive at the fully relativistic high gain dispersion relation

$$D(\omega,k_+) = \frac{\omega_b^2}{2} \left[\frac{\Omega_o}{ck_o}\right]^2 Q(\omega,k), \tag{75}$$

where

$$Q(\omega,k) = S(\omega,k) + \frac{c^2k^2}{\omega_b^2} \frac{\chi_\gamma^2(\omega,k)}{1 + \chi(\omega, k)}.$$

Again, we take a monoenergetic electron beam represented by the distribution function

$$g_o = \frac{u_z}{u} \delta(u - u_o) \tag{76}$$

where u_o is the total beam momentum. For such a beam we find that

$$\chi(\omega,k) = -\frac{\omega_b^2/(\gamma_{zo}^2 \gamma_o)}{(\omega - v_{zo} k)^2},$$

$$\chi_\gamma(\omega,k) = -\frac{\omega_b^2}{\gamma_o^2} \frac{(k - v_{zo}\omega/c^2)}{k(\omega - v_{zo} k)^2},$$

$$S(\omega,k) = -\frac{(\omega^2 - c^2k^2)}{\gamma_o^3(\omega - v_{zo} k)^2},$$

$$Q(\omega,k) = -\frac{D(\omega,k)}{\gamma_o^3(\omega - v_{zo}k)^2(1 + \chi(\omega,k))},$$

$$D(\omega,k) = \omega^2 - c^2k^2 - \omega_b^2/\gamma_o,$$

and the dispersion relation becomes

$$D(\omega,k_+) = -\frac{\omega_b^2}{2\gamma_o^3} \left[\frac{\Omega_o}{ck_o}\right]^2 \frac{D(\omega,k)}{[(\omega - v_{zo}k)^2 - \omega_b^2/(\gamma_{zo}^2 \gamma_o)]}, \tag{77}$$

where $\gamma_o = \gamma(u_o)$, $v_{zo} = v_z(u_o)$, and $\gamma_{zo} = \gamma_z(u_o)$.

Note that in the absense of the pump, $\Omega_o = 0$, we recover the uncoupled dispersion relations (27) for both the electromagnetic and electrostatic waves. In the presence of the pump, however, these two modes are coupled. Since the electromagnetic waves in the presence of the pump field approximately satisfy the pump free dispersion relation $D(\omega, k_+) \approx 0$, we can replace $D(\omega, k)$ on the right hand side of Eq. (77) by $-2kk_oc^2$. The dispersion relation in (77) may now be re-cast into the form

$$[k - (k_o + K)]\,[k - (k_o - K)]\,[k - (\omega/v_{zo} + \kappa)]\,[k - (\omega/v_{zo} - \kappa)] = -\alpha^2 k_o k, \quad (78)$$

where

$$K \equiv \left[\frac{\omega^2}{c^2} - \frac{\omega_b^2}{\gamma_o c^2}\right]^{1/2} > 0.$$

$$\kappa \equiv \omega_b/(v_{zo}\,\gamma_{zo}\,\gamma_o^{1/2}),$$

$$\alpha^2 \equiv \frac{\omega_b^2}{\gamma_o^3 v_{zo}^2}\left[\frac{\Omega_o}{ck_o}\right]^2 = (\xi\beta_{o\perp}\,k_o)^2,$$

$$\beta_{o\perp} = \frac{\Omega_o}{\gamma_o v_{zo} k_o},$$

and

$$\xi = \left[\frac{\omega_b}{\sqrt{\gamma_o}\,ck_o}\right].$$

We may now discern two limits for the solution of (78), depending upon the pump strength.

(a) *Weak-pump regime*

When the pump amplitude is smaller than a critical value, which we shall determine below, we may take the interacting longitudinal and transverse waves to be approximately nor-.

mal modes of the system. The positive-energy, fast space-charge mode of the beam is described by $k \simeq \omega/v_{zo} - \kappa$, while the negative-energy slow space-charge wave has $k \simeq \omega/v_{zo} + \kappa$. It is the interaction of the slow wave with the pump that leads to instability of the backscattered electromagnetic waves. The coupling of the negative-energy space-charge wave and the transverse electromagnetic wave is depicted in Fig. 5. Thus, in the case of a weak pump we can set

$$k = k_o + K + \delta k = \omega/v_{zo} + \kappa + \delta k; \tag{79}$$

where $|\delta k| << |k_o + K|$, $k_o << K$, $\omega/v_{zo} >> \kappa$ and $K \simeq \omega/v_{zo}$. Substituting Eq. (79) into (78) we find that the spatial growth rate is, for a highly relativistic beam,

$$\delta k = -i\frac{\alpha}{2}\sqrt{\frac{k_o}{\kappa}} = -\frac{i}{2}\beta_{o\perp}(\gamma_{zo}\xi)^{1/2}k_o. \tag{80}$$

The result (80) has been previously found by Sprangle *et al.* (1975), Kwan *et al.* (1977), Kroll and McMullin (1978), and Sprangle and Drobot (1978). This result is found under the assumption $|\delta k| << 2\kappa$, which leads to the constraint upon the pump amplitude

$$\beta_{0\perp} << \beta_{\text{crit}} \equiv 4\left(\frac{\xi}{\gamma_{zo}^3}\right)^{1/2}. \tag{81}$$

The difference between the phase velocity of the longitudinal wave and the axial beam velocity is

$$v_{ph} - v_{zo} = -\Delta v = -\frac{\xi}{2\gamma_{zo}^3}c.$$

Using this result in the efficiency expression of Eq. (46), we find (Kwan *et al*, 1977; Sprangle and Drobot, 1978)

$$\eta = \xi/\gamma_{zo}, \tag{82}$$

with the corresponding saturated field amplitude, from Eqs. (47) and (48), of

$$|\mathbf{E}|_{sat} = \frac{m_o c^2}{|e|}k_o\frac{\gamma_o}{\sqrt{\gamma_{zo}}}\xi^{3/2}. \tag{83}$$

The monenergetic beam assumption is valid if the axial thermal velocity of the beam V_{th} is much less than $\Delta v = v_{zo} - v_{ph}$, so that the wave is not resonant with any beam particles (see Fig. 3). Since $E_{th} = \gamma_o \gamma_{zo}^2 m_o c\ V_{th}$ for relativistic beams, the thermal energy spread must satisfy the requirement that

$$\frac{E_{th}}{E_o} << \frac{\xi}{2\gamma_{zo}} = \frac{\eta}{2} \tag{84}$$

(b) *Strong-Pump Regime*

In the weak-pump regime, where the longitudinal wave satisfies $1 + \chi(\omega,k) \simeq 0$, we see from Eq. (74) that the magnitude of the scalar potential $\tilde{\phi}(z)$, owing to charge separation, is much greater than the magnitude of the ponderomotive potential $\tilde{\phi}_{pond}(z)$. Thus the space-charge collective effects dominate the interaction. When the pump amplitude is sufficiently high, however, the ponderomotive forces may modify the electrostatic wave dispersion so that $|\chi(\omega,k)| << 1$. In this case the space-charge collective effects are negligible. Thus to consider the strong-pump regime we take

$$|\delta k| >> 2\kappa \tag{85}$$

in Eq. (79). Substituting (79) into (78) the dispersion relation reduces to

$$(\delta k)^3 = -\frac{\xi^2 \beta_{o\perp}^2 k_o^3}{2} \tag{86}$$

and the unstable root is (Kroll and McMullin, 1978; Sprangle and Drobot, 1978)

$$\delta k = \left(\frac{1 - i\sqrt{3}}{2^{4/3}}\right) (\xi \beta_{0\perp})^{2/3} k_o . \tag{87}$$

From the result in (87), we see that the strong-pump condition (85) is the inverse of (81), *i.e.*,

$$\beta_{0\perp} >> \beta_{crit} = 4(\xi/\gamma_{zo}^3)^{1/2}. \tag{88}$$

The phase velocity of the unstable longitudinal wave is

$$v_{ph} = \frac{\omega}{Re(k)} = v_{zo} - \frac{Re(\delta k)}{k}$$

$$= v_{zo} - \frac{1}{2^{1/3}} \frac{(\xi\beta_{0\perp})^{2/3} c}{4\gamma_{zo}^2} . \tag{89}$$

From Eqs (46) and (48) we find that the corresponding efficiency and saturated amplitude are given by

$$\eta = \left(\frac{\xi\beta_{a\perp}}{4} \right)^{2/3} \tag{90}$$

and

$$|\mathbf{E}|_{sat} = \frac{m_o c^2}{|e|} k_o (\xi^4 \gamma_o^3 \beta_{o\perp}/4)^{1/3} , \tag{91}$$

respectively (Sprangle and Drobot, 1978). The energy spread requirement to use a cold beam distribution is given by

$$\frac{E_{th}}{E_o} << \frac{1}{2} \left(\frac{\xi\beta_{0\perp}}{4} \right)^{2/3} = \frac{\eta}{2} . \tag{92}$$

The general behavior of the growth rate and efficiency as a function of $\beta_{a\perp}$ (pump strength), in both the strong and weak-pump regimes, are shown schematically in Figure 6. In the weak pump regime the spatial growth rate is proportional to the pump strength, while the efficiency is independent of the pump. For the strong pump case both the growth rate and the efficiency vary as $\beta_{a\perp}^{2/3}$. Higher growth rates and efficiencies, therefore, make the strong pump limit a more attractive mechanism for generating high frequency radiation. In Table I we summarize the results of analyses of all the cases 1-3 for a highly relativistic beam ($v_z \simeq c$).

IV. DISCUSSION: A VISIBLE-LIGHT FREE ELECTRON LASER

In this section we apply the theory to a specific example of a high-power FEL at optical wavelengths. We first note two considerations important for high-current beams: (i) the effect of the beam itself on the pump magnetic field; and (ii) the induced energy spread in the beam due to its self electrostatic potential. These considerations place an upper limit in the beam current.

With regard to (i) we note that the beam equilibrium motion in the external pump field contains a transverse velocity component $\beta_{o\perp}c$. The beam motion, therefore, induces a spatially periodic, diamagnetic field that tends to oppose the applied pump field. It may easily be shown that with an equilibrium distribution

$$g_o(\alpha,\beta,u) = n_o\frac{u_z}{u}\,\delta(\alpha)\delta(\beta)\delta(u-u_o),$$

the diamagnetic field amplitude B_d is of order

$$|B_d| \sim \xi^2 B_o,$$

where ξ is the beam strength parameter defined above: $\xi = \omega_b/(\sqrt{\gamma_o}ck_o)$. Thus, in order to neglect the perturbations to the equilibrium orbit owing to the diamagnetic field, we require $\xi \ll 1$.

With regard to point (ii), we note that an un-neutralized electron beam has an inherent energy spread owing to the variation of the electrostatic potential within the beam. For a cylindrical beam of radius r_o the potential difference between the central axis to the outer edge of the beam is

$$\Delta\phi = \pi|e|n_o r_o^2.$$

Associated with this potential difference is a kinetic energy change across the beam, given by

$$\Delta E = \Delta\gamma m_o c^2 = |e|\Delta\phi.$$

This variation in kinetic energy may be interpreted as indicating a thermal energy spread in the beam, of relative magnitude

$$\frac{\Delta E}{E_o} = \frac{|e|\Delta\phi}{(\gamma_o - 1)m_o c^2} \simeq \left[\frac{\xi k_o r_o}{2}\right]^2,$$

where we have taken $\gamma_o >> 1$. For sufficiently high beam densities this inherent energy spread may invalidate the cold-beam approximation.

As noted above, the strong-pump scattering require (case 3b) is characterized by the highest spatial growth rates and efficiencies, and is thus the most promising case for application. Therefore, we shall choose parameters appropriate to this regime.

We take a periodic magnetic pump field of period $l = 0.75$ cm and amplitude $B = 7.5$ kG. The electron beam current I_o is taken to be 2 kA, with beam radius 0.1 cm and energy 45 Mev ($\gamma_o = 90$). The transverse velocity induced by the pump is

$$v_{o\perp} = \beta_{o\perp} c = |e|B_o/\gamma_o m_o c k_o = 6.0 \times 10^{-3} c,$$

where $k_o = 2\pi/l$. The radian plasma frequency of the beam is $\omega_b = 2.0 \times 10^{11}$ sec^{-1}, and the pump strength parameter $\xi = \omega_b/(\sqrt{\gamma_o} c k_o) = 8.4 \times 10^{-2}$. The longitudinal Lorentz factor $\gamma_{zo} = 80$, giving $\beta_{crit} = 4(\xi/\gamma_{zo}^3)^{1/2} = 1.62 \times 10^{-3} << \beta_{o\perp}$, verifying that these parameters are indeed characteristic of the strong-pump regime. The wavelength of the scattered wave is $\lambda_s = l/2\gamma_{zo}^2 = 0.58$ μm, in the visible region of the spectrum. From the formulae of Case 3b, summarized in Table I, we find a spatial growth rate $|-\mathrm{Im}k| = \sqrt{3}(\xi\beta_{o\perp}/4)^{2/3} k_o = 3.6 \times 10^{-2}$ cm^{-1}, corresponding to an e-folding length of 28 cm. Thus, very high gains may be achieved in a single pass over a total distance of several meters. The single-pass efficiency is given by $\eta = (\xi\beta_{o\perp}/4)^{2/3} = 0.25\%$. With regard to the constraints on the current imposed by the neglect of the induced diamagnetic field and the beam quality necessary to apply the cold-beam approximation, the first of these is well satisfied as $\xi^2 << 1$, and the second is marginally satisfied as $\Delta E/E_o = (\xi r_o k_o/2)^2 = 0.12\%$, to be compared with the efficiency of 0.25%. The radiated power P_s, at 0.58 μm, is given by $P_s = \eta I_o E_o = 230$ MW. The parameters of this example are summarized in Table II.

Finally, we note that it is in principle possible to increase substantially the single-pass efficiency by recovering part of the beam energy with a depressed collector and by continuously

decreasing the phase velocity of the pondermotive wave in order to delay trapping, which saturates the process. The decrease in phase velocity can be achieved by adiabatically decreasing the wavelength of the pump field. In this way energy will be extracted from the beam until a greater degree of thermalization is attained, with correspondingly higher efficiency. Extrapolating the results of present technology to the FEL, we might expect the combination of beam recovery and phase-velocity tapering to yield increases of roughly an order of magnitude in the single-pass efficiency. As of this writing (mid-1978), however, detailed analyses of these effects have not been completed; these will be the subjects of continued investigations.

V. LABORATORY EXPERIMENTS

Data on laboratory studies of stimulated scattering from relativistic electrom beams are summarized in Table III. The five experiments listed divide naturally into two regimes; i) the low-gain regime investigated using the superconducting linear accelerator at Stanford University (examples 1 and 2 in the table); and ii) the high-gain collective regime investigated using intense relativistic electron beam accelerators at the Naval Research Laboratory and at Columbia University (examples 3, 4, and 5 in the table).

The low-gain regime studies were characterized by relatively high electron energies (24-43 MeV) and correspondingly short output wavelength (3-11 μm). Line broadening of spontaneous emission was dominated by finite length effects rather than by spread in electron energy since $l/L > 2E_{th}/E_o$ (see Eq. 38). The current was relatively small (0.1-2.6 A) corresponding to a low value of amplitude gain; in an amplifier experiment (example 1), $G_L = 0.035 << 1$. In an oscillator experiment (example 2), a peak output power of 7 kW was realized which corresponded to 0.006% of the energy in the electron beam; average output power was 0.36 watts.

In contrast, the intense beam studies had lower electron energy (.86-2 MeV) and correspondingly longer output wavelengths (400-1500 μm). Line broadening was dominated by electron energy spread since $2E_{th}/E_o > l/L$. (E_{th} was estimated to equal the electrostatic energy shear across the beam.) The current was much larger (5-40 kA) making possible the participation of collective electron beam modes in the stimulated scattering process, and resulting in large gain; in one superradiant oscillator experiment (example 3), the measured amplitude gain was $G_L > 2$. In a second superradiant oscillator experiment (example 3), the strength of the pump was increased to ensure saturation of wave growth, and a peak power output of 8 MW was measured; this was three orders of magnitude larger than the saturated peak power in

the low-gain oscillator experiment, corresponding both to larger peak beam power and to a somewhat larger efficiency (0.2%). As yet, there is no continuous power capability in the intense beam experiments, the experiments being characterized by a single electron pulse of 10-50 nsec duration.

In the intense beam experiments two types of pump wave were investigated: a magnetic wiggler (examples 4 and 5) as was used in the low gain experiments and, alternatively, a powerful electromagnetic wave (example 3). The intense beam experiments also had an externally imposed uniform axial magnetic field that was large enough so that magnetic resonances in the output power were observed.

Some appreciation for the significance of the experimental results listed in Table III may be obtained by comparing the peak powers achieved with other existing capabilities for generating high-power coherent radiation. Two distinct technologies are currently being used. Conversion of electron kinetic energy into microwaves by coupling beam waves to electromagnetic waves on a slow-wave structure is a highly developed technology at centimeter and millimeter wavelengths. This technology is characterized by numerous device types which can be scaled or tuned to cover a wide frequency range. As shown by the solid line in Fig. 7, however, the available power decreases rapidly as wavelength is shortened.

At optical and near infrared wavelengths, the technology of lasers based on atomic and molecular transitions has been successful in generating very high power using a variety of media. The number of atomic or molecular transitions which result in laser action are limited, however, and high power is generally available only in narrow bands. Some tunable molecular systems do exist (*e.g.* dye lasers) but these are restricted in their power output because large average power operation results in decomposition of the active medium (*i.e.*, the dye).

In contrast, the preliminary results obtained with the free electron laser point to the possibility of developing high-power, tunable systems operating over a wavelength range extending from the millimeter to the optical. The data points indexed as 3 and 4 in Fig. 7 correspond to the intense beam scattering results listed in Table III as examples 3 and 4, respectively. The low-gain oscillator result obtained with the Stanford superconducting linear accelerator (example 2 in Table III) is shown by the third data point. A more detailed description of the various stimulated scattering experiments follows.

a) *Experiments in the low gain regime at infrared wavelengths.*

The experimental arrangement corresponding to example 1 in Table III is depicted in Fig. 8. The output from a 50 kW, 10.6 μm laser was amplified upon interacting with a beam of 24 MeV electrons passing through a wiggler magnetic field with period $l = 3.2$ cm. The axial electron energy in the interaction region was evidently $\gamma_z = 39$ to satisfy $l/2\gamma_{z0}^2 = \lambda_s$; this may be compared with a total energy of $\gamma_0 = 48$.

As shown by Kroll and McMullin (1978), the experimental parameters indicate that the interaction took place in the low gain, tenuous cold beam regime; thus, the expressions for Case 1 in Table I are applicable. Gain was measured to be a linear function of current for $5 < I < 70$ mA. The maximum energy gain measurement was 7% corresponding to a stimulated emission of 60 keV/electron or an efficiency of 0.25%. The measured gain is somewhat larger than, but is of the same order as, the gain calculated from the expression for $-\int_0^L Im(k)\,dz$ in case 1 of Table I when this is multiplied by a filling factor of 2×10^{-2}, which is the ratio of the electron beam area to the area of the applied 10.6 μm radiation. The measured efficiency approaches the theoretical value of $\pi/k_0 L = 0.31\%$, indicating that the process was close to saturation.

The spontaneous power emitted at 10.6 μm is plotted as a function of electron energy in Fig. 9 together with gain measured when the CO_2 laser radiation was applied. The full width at the $1/e$ points of the spontaneous power curve is 0.4% which agrees well with a theoretical broadening of 0.3% due to the finite length of the interaction region. The shape of the gain curve showing inverse dependence on the first derivative of the spontaneous emission curve also agrees with theory.

The experimental arrangement corresponding to the oscillator in example 2 of Table III is shown in Fig. 10. The same helical magnet undulator was used as with the amplifier experiment shown in Fig. 8. However, energy of the electrons was increased to 43 MeV so that stimulated emission occurred at the shorter wavelength of 3.4 μm. The electrons are formed into bunches only 1.3 mm in length with a spacing between bunches of approximately 25 m. The spacing between the resonator mirrors is carefully adjusted so that the round-trip bounce time for the 3.4 μm radiation is equal to the time interval between electron pulses entering the cavity.

The emission spectrum of the laser oscillator above threshold is shown together with the spectrum of the spontaneous radiation emitted by the electron beam in Fig. 11. The 0.9% linewidth of the spontaneous emission should be compared with theoretical linewidth of 0.6% due to the finite length of the helical undulator. Lasing in the optical resonator reduces linewidth to 0.2%.

The peak output power was 7 kW corresponding to 0.006% of the beam energy. Assuming this experiment to be in the same parameter regime as the amplifier experiment of Elias *et al*, one would expect that the applicable theoretical efficiency would again be $\pi/k_0 L = 0.3\%$. Perhaps the lower experimental efficiency was due to a choice of output window transmissivity that was not optimum.

b) *Submillimeter generation in the high-gain, collective regime with an electromagnetic pump.*

The experimental arrangement corresponding to example 3 in Table III is shown schematically in Fig. 12. A voltage pulse (−2 MV, 50 ns) was applied to a cold cathode immersed in a uniform axial magnetic field $<B> \approx 13$kG. A resultant annular electron beam was injected into a drift tube along the lines of $<B>$. Electrostatic forces reduced electron kinetic energy so that $\gamma_0 = 3.9$.

At one point in the drift tube, the electron beam was passed through a nonadiabatic perturbation in the applied magnetic field which converted a large fraction of the electron streaming energy into energy transverse to the axis of the drift tube. The electrons with large transverse energy then reacted unstably with an electromagnetic mode of the drift tube (cyclotron maser process as described in Hirshfield and Granatstein (1977)) and produced a 2 cm pump wave having a power of 10-100 MW. This pump wave was reflected off a metallic plate and travelled back up the drift tube toward the cathode. When the pump wave encountered the cold streaming electrons near the cathode, stimulated scattering occurred resulting in backscattered submillimeter waves.

The submillimeter output radiation was monitored through an array of metallic tubes passing through the reflecting plate. Each tube passed the radiation through wave filters and into a pyroelectric detector. The submillimeter output power was optimized by varying both the axial position of the magnetic modulator and the level of $<B>$. The total submillimeter radiation incident on the metallic reflector was shown to be peaked at $\lambda_s = 400\ \mu$m and have a power of 1 MW.

Dependence of the submillimeter radiation on the position of the magnetic modulator is shown in Fig. 13. As the modulator was moved downstream from the cathode, the scattering

region L_2 was lengthened while simultaneously shortening the region L_1 in which the pump wave is generated. Thus, one expected an initial increase in the submillimeter output as the scattering became stronger followed by a decreasing submillimeter output as the pump wave is weakened. In Fig. 13, a plot of submillimeter power vs. L_2 shows the expected behavior with the submillimeter output having a maximum at $L_2 = 30$ cm. The rising portion of the curve in Fig. 13 has a slope indicating an amplitude gain for the stimulated scattering of $G_L > 2$ or equivalently a spatial growth rate of $\mathrm{Im}(k) > 0.02\ \mathrm{cm}^{-1}$.

Only a lower bound is determined by the data of Fig. 13 since the pump wave amplitude decreases as L_2 is made larger. This lower bound on spatial growth rate may be compared with the theoretical value $-\mathrm{Im}(k) = 0.04\ \mathrm{cm}^{-1}$ calculated from the expression for case 3a in Table I, and using the expression for $\beta_{o\perp}$ from Sprangle, *et al.*, (1975) (*viz.*, $\beta_{o\perp} = |e|\mathcal{E}_o/\gamma_o m_o(\omega_o - <\Omega>/\gamma_o)$ where $\mathcal{E}_o$ is the electric field and $<\Omega> = |e|<B>/m_o c$. For the parameters of the experiment in Fig. 10, we calculate $\beta_{o\perp} = .02$ and $\beta_{crit} = 0.4$ while $E_{th}/E_o = 0.04$ and $\xi/\gamma_{zo} = .13$; thus, the condition $\beta_{o\perp} << \beta_{crit}$ is well satisfied while $E_{th}/E_o << \xi/\gamma_{zo}$ is marginally satisfied. Hence, one is justified in using the theoretical expressions for the high gain collective scattering regime of case 3a.

Dependence of the submillimeter power on $<B>$, the solenoidal magnetic field strength, is shown in Fig. 14. A maximum is seen at $<B> = 13$ kG with a half-power width of 3 kG. The pump wave power at $\lambda_s = 2$ cm was relatively constant in the range 10 kG $< <B> <$ 16 kG so that the behavior depicted in Fig. 14 corresponds to resonant interactions in the stimulated scattering process.

The experimental configuration in Fig. 12 is limited by the fact that both pump wave generation and stimulated scattering occur in the same electron beam. This does not allow for

separate optimization of each process and complicates interpretation of the experimental results. To overcome these disadvantages, the new experimental configuration in Fig. 15 is being assembled at NRL. Two synchronized pulsed-power systems are being employed. The pulse-forming network from a 600 kV flash x-ray system (peak power = 3.6 GW) will be used to drive an S-band magnetron that will furnish a multi-gigawatt pump wave at $\lambda_o = 9.4$ cm.

A larger 2.5 MV accelerator (peak power 25 GW) will provide the annular electron beam ($A_b = 7$ cm^2) in which stimulated scattering may take place. The backscattered output radiation is expected to be at $\lambda_s = 1700$ μm. Given the magnitude of microwave power available from the magnetron, this stimulated scattering experiment is expected to be the first operating in the strong pump limit ($\beta_{o\perp} > \beta_{crit}$). The expressions for case 3b in Table I are applicable and using them one calculates a spatial growth rate $-\mathrm{Im}(k) = 0.4$ cm^{-1} and an efficiency $\eta = 11\%$.

The investigations of stimulated scattering using electromagnetic pump waves are of practical importance since pump wavelengths can be realized which are much shorter than those which are possible with a magnetic wiggler. Thus for a given output wavelength there is a reduced requirement on accelerator voltage. However, as is apparent from the discussion above, the production of strong electromagnetic pump waves is far more difficult technologically than the production of a magnetic wiggler field.

c) *Experiments in the high-gain, collective regime with a magnetic wiggler*

The experimental arrangement corresponding to example 4 in table III is depicted in Fig. 16. As in part b) above an intense electron beam of annular cross-section was propagated axially down a drift tube along the lines of a solenoidal magnetic field $<B>$. However, in this case, a ripple component was added to the solenoidal field over a distance typically $L = 40$ cm. The radial component of the ripple field B_o could be varied from 0 to 500 G, and ripple periods

of 6 mm and 8 mm were used. From the parameters in table III, one calculates $\beta_{o\perp} = 0.01$, $\beta_{crit} = 0.35$, and $\xi/\gamma_{zo} = 0.03$ while $E_{th}/E_o = 0.02$. Thus $\beta_{o\perp} << \beta_{crit}$ is well satisfied, but $E_{th}/E_o \lesssim \xi/\gamma_{zo}$ rather than $E_{th}/E_o << \xi/\gamma_{zo}$. One therefore expects operation to have been marginally in the high-gain, collective regime.

The emission spectrum was resolved using a grating spectrometer of special design. A typical spectrum is shown in Fig. 17. As shown in the figure, it was found that the emission spectrum consisted of peaks at two distinct wavelengths which were interpreted as corresponding to the frequencies

$$\omega_{S1} = (1 + \beta_{zo})\gamma_{zo}(\gamma_{zo}k_o v_{zo} - \omega_b/\gamma_o^{1/2})$$

and

$$\omega_{S2} = (1 + \beta_{zo})\gamma_{zo}^2(v_{zo}k_o - |e| <B>/m_o c\gamma_o).$$

The shorter wavelength peak at ω_{S1} would then correspond to a stimulated scattering process involving a space charge beam mode as an idler. The longer wavelength peak at ω_{S2} would correspond to a scattering process with a cyclotron mode idler. Indeed it was found that the longer wavelength peak would be tuned in frequency by changing $<B>$, while ω_{S1} remained constant.

Marshall *et al.* (1977) measured power in the wave at ω_{S2} to be 8 megawatts. This was found experimentally to represent a saturated power level (Gilgenbach, 1978) and corresponds to an efficieny of 0.2%. The theoretical analysis presented in this paper does not apply to the case of a cyclotron mode idler. The power measured at ω_{S1} was 2 MW but this was not established to be a saturated value.

The experiment of Marshall *et al.* (1977) shown in Fig. 16 functioned as a superradiant oscillator. Experiments have now been carried out (McDermott *et al*, 1978) using mirrors to

form a quasi-optical cavity. The experimental arrangement corresponding to example 5 in Table III is shown in Fig. 18. The separation between the mirrors was 1.5 m while the time duration of the electron beam pulse was approximately 40 ns so that radiation would execute only 4 round-trip bounces between the mirrors while the beam was on. Nevertheless, evidence of lasing was observed with coherence of the radiation measured as $\Delta\lambda_s/\lambda_s = 2\%$ compared with $\Delta\lambda_s/\lambda_s \gtrsim 10\%$ for the superradiant oscillator. According to McDermott *et al* (1978), the stimulated scattering process involved a space charge wave idler, while scattering from the cyclotron idler was damped.

VI. CONCLUSIONS

Free electron lasers based on stimulated scattering from intense electron beams hold the promise of making available very-high-power, moderately coherent, widely tunable sources over a wavelength range from millimeters down to optical wavelengths and beyond. This paper contains design examples of a 1700 μm laser with peak power of several gigawatts operating at 11% efficiency and a 0.58 μm laser with power of hundreds of megawatts operating with 0.25% efficiency.

Clearly, much investigation will be required before this potential can be fully evaluated. The experiments which have been carried out to date give support to the linear theory, but carefully designed experimental investigations of the nonlinear regime still remain to be executed.

Also, accelerator technology studies are required to evaluate the average power potential. In connection with free electron lasers based on linear accelerators, the use of storage rings is under study. For free electron lasers based on intense electron beams, there is great interest in

the studies which have been initiated on repetitively pulsing intense beam accelerators and recovering energy in the spent electron beam through depressed-collector techniques.

The theoretical studies, while presently more advanced than the experiments, are also far from complete. It should be of great value to relax some of the model idealizations, and include consideration of oblique angle scattering, energy shear in the electron beam, the presence of a uniform magnetization, and finite transverse beam geometry. Most important of all, the study of axially nonuniform systems (*e.g.*, tapering the periodicity of the magnetic wiggler) may indicate efficiencies greatly enhanced over those calculated above for uniform systems.

VII. ACKNOWLEDGMENTS

The authors wish to express their appreciation to R.K. Parker and I.B. Bernstein for useful discussions. Also, R.K. Parker provided figures 7 and 15.

APPENDIX

We indicate briefly here the details of the derivation of Eqs. (24) from Eq. (20), within the context of the distribution function (23). Substituting the expression for $\tilde{g}^{(1)}$ given in Eq. (16) with $g^{(0)}(\alpha, \beta, u) = n_o \delta(\alpha)\, \delta(\beta)\, g_o(u)$ into Eq. (20) and integrating by parts gives

$$\begin{bmatrix} \tilde{J}_{\pm}(z) \\ \tilde{J}_{z}(z) \end{bmatrix} = \frac{|e|\, n_o}{m_o} \int_o^{\infty} \frac{u}{\gamma(u)} \left\{ \left[\frac{\partial}{\partial \alpha} + i \frac{\partial}{\partial \beta} \right] \left[\begin{bmatrix} p_{\pm}(\alpha, \beta, z) \\ p_{z}(\alpha, \beta, u, z) \end{bmatrix} \frac{\tilde{G}_{+}(\alpha, \beta, u, z)}{p_{z}(\alpha, \beta, u, z)} \right] \right.$$

$$+ \left[\frac{\partial}{\partial \alpha} - i \frac{\partial}{\partial \beta} \right] \left[\begin{bmatrix} p_{\pm}(\alpha, \beta, z) \\ p_{z}(\alpha, \beta, u, z) \end{bmatrix} \frac{\tilde{G}_{-}(\alpha, \beta, u, z)}{p_{z}(\alpha, \beta, u, z)} \right]$$

$$\left. - \begin{bmatrix} p_{\pm}(\alpha, \beta, z) \\ p_{z}(\alpha, \beta, u, z) \end{bmatrix} \frac{\tilde{G}_{z}(\alpha, \beta, u, z)}{p_{z}(\alpha, \beta, u, z)} \frac{\partial}{\partial u} \right\}_{\alpha=\beta=0} g_o(u)\, du \qquad \text{(A1)}$$

In order to evaluate the current densities in (A1) the following relations are needed:

$$p_{\pm}(\alpha, \beta, z) = p_x \mp i p_y = \alpha \mp i\beta - \frac{|e|\, B_o}{c\, k_o}\, e^{\pm i k_o z};$$

$$p_{z}(\alpha, \beta, u, z) = \left[u^2 - \left[\alpha + \frac{|e|}{c} A_{ox}(z) \right]^2 - \left[\beta + \frac{|e|}{c} A_{oy}(z) \right]^2 \right]^{1/2};$$

$$u_{0\perp} = \frac{|e| B_o}{c\, k_o} = m_o\, \Omega_o / k_o,\ \Omega_o = |e|\, B_o / m_o c;$$

$$p_{\pm}(\alpha, \beta, u, z)_{\alpha=\beta=0} = -u_{0\perp}\, e^{\mp i k_o z};$$

$$p_{z}(\alpha, \beta, u, z)_{\alpha=\beta=0} = \sqrt{u^2 - u_{o\perp}^2} = u_{z}(u) = \gamma(u)\, m_o\, v_{z}(u);$$

$$\left[\frac{\partial}{\partial \alpha} + i \frac{\partial}{\partial \beta} \right] p_{\pm}(\alpha, \beta, z)_{\alpha=\beta=0} = \begin{bmatrix} 2 \\ 0 \end{bmatrix};$$

$$\left[\frac{\partial}{\partial \alpha} - i \frac{\partial}{\partial \beta} \right] p_{\pm}(\alpha, \beta, z)_{\alpha=\beta=0} = \begin{bmatrix} 0 \\ 2 \end{bmatrix};$$

$$\left\{\frac{\partial}{\partial\alpha} \pm i\frac{\partial}{\partial\beta}\right\} p_z(\alpha, \beta, u, z)\Big|_{\alpha=\beta=0} = \frac{u_{0\perp}}{u_z(u)}\, e^{\pm ik_o z};$$

$$\left\{\frac{\partial}{\partial\alpha} \pm i\frac{\partial}{\partial\beta}\right\} \tau(\alpha, \beta, u, z', z)\Big|_{\alpha=\beta=0} = \pm i\frac{\Omega_o/\gamma(u)}{u_z(u)\, k_o^2 v_z^2(u)}\left\{e^{\pm ik_o z'} - e^{\pm ik_o z}\right\};$$

$$\left\{\frac{\partial}{\partial\alpha} \pm i\frac{\partial}{\partial\beta}\right\} M(\alpha, \beta, u, z', z)\Big|_{\alpha=\beta=0}$$

$$= \pm \frac{\Omega_o/\gamma(u)}{k_o^2 v_z^2(u)} \frac{e^{-i\frac{\omega}{v_z(u)}(z'-z)}}{v_z(u)\, u_z(u)}\left\{(\omega \mp v_z(u)\, k_o)\, e^{\pm ik_o z'} - \omega e^{\pm ik_o z}\right\};$$

$$\left\{\frac{\partial}{\partial\alpha} \pm i\frac{\partial}{\partial\beta}\right\} \frac{p_\pm(\alpha, \beta, z)}{p_z(\alpha, \beta, u, z)}\Big|_{\alpha=\beta=0} = \frac{1}{u_z(u)}\left\{2 + (u_{o\perp}/u_z(u))^2\right\};$$

$$\left\{\frac{\partial}{\partial\alpha} \pm i\frac{\partial}{\partial\beta}\right\} \frac{p_\mp(\alpha, \beta, z)}{p_z(\alpha, \beta, u, z)}\Big|_{\alpha=\beta=0} = \frac{u_{0\perp}^2}{u_z^3(u)}\, e^{\pm 2ik_o z};$$

$$\left\{\frac{\partial}{\partial\alpha} \pm i\frac{\partial}{\partial\beta}\right\} \tilde{G}_\pm(\alpha, \beta, u, z)\Big|_{\alpha=\beta=0} = \mp \frac{|e|\,\omega}{2c} \frac{\Omega_o/\gamma(u)}{k_o^2 v_z^2(u)} \frac{(e^{\pm ik_o z} - 1)}{u_z(u)}\, \tilde{A}_\pm(0)\, e^{i\omega z/v_z(u)};$$

$$\tilde{G}_z(\alpha, \beta, u, z)\Big|_{\alpha=\beta=0} = \frac{-\gamma(u)\, m_o|e|}{2u\, v_z(u)}\, e^{i\omega z/v_z(u)}$$

$$\int_o^z e^{\frac{-i\omega z'}{v_z(u)}}\left\{v_z(u)\frac{\partial\tilde{\phi}(z')}{\partial z'} + i\frac{\omega}{ck_o}\frac{\Omega_o}{\gamma(u)}\left[\tilde{A}_+(z')\, e^{ik_o z'} + \tilde{A}_-(z')\, e^{-ik_o z'}\right]\right\} dz'.$$

With the above relations it becomes straightforward to derive Eqs. (24).

REFERENCES

Bernstein, I.B., and Hirshfield, J. L. (1978). *Phys. Rev. Lett.* **40**, 761-764.

Buzzi, J. M., Doucet, H. J., Etlicher, B., Haldenwang, P., Huetz, A., Lamain, H., and Rouille, C. (1977). *Journal de Physique Lettres* **38**, L397-L399.

Coleman, P. D. (1961) in *Advances in Quantum Electronics* (Columbia Univ. Press, New York).

Colson, W. B. (1976). *Phys. Lett. 59A*, 187-190.

Colson, W. B. (1977) in *Physics of Quantum Electronics* **5** (S. Jacobs, M. Sargent III, and M. Scully, eds.), 152-196.

Deacon, D. A. G., Elias, L. R., Madey, J. M. J., Ramian, G. J., Schwettman, H. A., and Smith, T. I. (1977). *Phys. Rev. Lett.* **38**, 892-894.

Drake, J. F., Kaw, P. K., Lee, Y. C., Schmidt, G., Liu, C. S., and Rosenbluth, M. N. (1974). *Phys. Fluids* **17**, 778-785.

DuBois, D. F., and Goldman, M. V. (1965) *Phys. Rev. Lett.* **14**, 544-546.

DuBois, D. F., and Goldman, M. V. (1967). *Phys. Rev.* **164**, 207-222.

Efthimion, P. C., and Schlesinger, S. P. (1977). *Phys. Rev. A* **16**, 633-639.

Elias, L. R., Fairbank, W. M., Madey, J. M. J., Schwettman, H. A., and Smith, T. I. (1976). *Phys. Rev. Lett.* **36**, 717-720.

Forslund, D.W., Kindle, J.M., and Lindman, E.L. (1973). *Phys. Rev. Lett.* **30**, 739-743.

Gilgenbach, R. M., Marshall, T. C., and Schlesinger, S. P. (1978). *Phys. Fluids* (to be published).

Gilgenbach, R.M. (1978), Ph.D. Thesis, Columbia University.

Gover, A., and Yariv, A. (1978). *Appl Phys.* (in press).

Granatstein, V. L. Herndon, M., Parker, R. K., and Schlesinger, S. P. (1974). *IEEE Trans. Microwave Theory Tech. MTT-22,* 1000-1005.

Granatstein, V. L., Schlesinger, S. P., Herndon, M., Parker, R. K., and Pasour, J. A. (1977). *Appl. Phys. Lett.* **30**, 384-386.

Granatstein, V. L., Sprangle, P., Parker, R. K., Pasour, J., Herndon, M., Schlesinger, S. P., and Seftor, J. L. (1976). *Phys. Rev. A* **14**, 1194-1201.

Granatstein, V.L., and Sprangle, P. (1977) *IEEE Trans. MTT-25*, 545-550.

Hasegawa, A. (1978) (Submitted for publication.)

Hasegawa, A., Mima, K., Sprangle, P., Szu, H. H., and Granatstein, V. L. (1976). *App. Phys. Lett.* **29**, 542-544.

Hirshfield, J.L., and Granatstein V.L. (1977), *IEEE Trans. MTT-25*, 522-527.

Hopf, F. A., Meystre, P., Scully, M. O., and Louisell, W. H. (1976a). *Optics Comm.* **18**, 413-416.

Hopf, F. A., Meystre, P., Scully, M. O., and Louisell, W. H. (1976b). *Phys. Rev. Lett.* **37**, 1342-1345.

Kapitza, P. L. and Dirac, P. A. M. (1933). *Proc. Cambridge Phil. Soc* **29** 297-300.

Kaw, P. K., and Dawson, J. M. (1971). *Phys. Fluids* **14**, 792-794.

Kroll, N. M., and McMullin, W. A. (1978) *Phys. Rev. A* **17**, 300-308.

Kwan, T., Dawson, J. M., and Lin, A. T. (1977). *Phys. Fluids* **20**, 581-588.

Lampe, M., Ott, E., and Walker, J. H. (1978). *Phys. Fluids* **21**, 42-54.

Lin, A. T., and Dawson, J. M. (1975). *Phys. Fluid* **18**, 201-206.

Madey, J. M. J. (1971). *J. Appl. Phys.* **42**, 1906-1913.

Madey, J. M. J., Schwettman, H. A., and Fairbank, W. M. (1973). *IEEE Trans. Nucl. Sci.* **20**, 980-983.

Manheimer, W. M., and Ott, E. (1974). *Phys. Fluids* **17**, 1413-1421.

Marshall, T. C., Talmadge, S., and Efthimion, P. (1977). *App. Phys. Lett.* **31**, 320-322.

McDermott, D. B., Marshall, T. C., and Schlesinger, S. P. Parker, R. K., and Granetstein, V. L. (1978). *Phys. Rev. Lett.* (to be published).

Miroshnichenko, V. I. (1975). *Sov. Tech. Phys. Lett.* **1**, 453-454.

Motz, H. (1951). *J. Appl. Phys.* **22**, 527-535.

Nishikawa, K. (1968). *J. Phys. Soc.* Japan **24**, 916-922.

Pantell, R. H., Soncini, G., and Puthoff, H. E. (1968). *IEEE J. Quantum Elect.* **4**, 905-907.

Parker, R.K., and Ury M. (1975), *IEEE Trans. NS22*, 983-988.

Pasour, J. A., Granatstein, V. L., and Parker, R. K. (1977). *Phys. Rev. A* **16**, 2441 -2446.

Perkins, F. W., and Kaw, P. K. (1971). *J. Geophys. Res.* **76**, 282-284.

Schneider, S., and Spitzer, R. (1974). *Nature* **250**, 643-645.

Silin, V. P. (1965). *Sov. Phys. JETP* **21**, 1127-1134.

Silin, V. P. (1967). *Sov. Phys. JETP* **24**, 1242-1247.

Sprangle, P., and Drobot, A. T. (1978). NRL Memo. Rept. 3587, *J. Appl. Phys.* (to be published).

Sprangle, P., and Granatstein, V. L. (1974). *Appl. Phys. Lett.* **25**, 377-379.

Sprangle, P. Granatstein, V. L., and Baker, L. (1975). *Phys. Rev.* **A12**, 1697-1701.

Sprangle, P., and Granatstein, V. L. (1978). *Phys. Rev. A* **17**, 1792-1793.

Sukhatme, V. P., and Wolff, P. W. (1973). *J Appl. Phys.* **44**, 2331 - 2334.

Walsh, J. E., Marshall, T. C., and Schlesinger, S. P. (1977). *Phys. Fluids* **20**, 709.

Table I — Summary of FEL Regimes

Free Electron Laser Regimes	Spatial Growth Rate, -Im(k)	Efficiency η	Scattered E-Field, $\lvert\mathbf{E}\rvert_{sat}$	Thermal Spread, E_{th}/E_o
Case 1: Low Gain, $-\int_o^L Im(k)\,dz \ll 1$ Tenuous - Cold Beam	$\left(\frac{\xi\beta_{o\perp}}{4}\right)^2 (k_o L)^3$ integrated over L	$\frac{\pi}{k_o L}$	$\frac{4.5}{\pi^2}\frac{m_o c^2}{\lvert e\rvert} k_o \gamma_o \beta_{o\perp}^{-1}\eta^2$	$\ll \eta$
Case 2: High Gain, $-Im(k)z \gg 1$ Tenuous-Warm Beam	$\frac{\sqrt{\pi}}{20}\left(\xi\beta_{o\perp}\frac{E_o}{E_{th}}\right)^2 k_o$	$\frac{1}{4\sqrt{2\pi}}\left(\frac{\delta u_w}{U_{th}}\right)^3 \frac{E_{th}}{E_o}$	$\frac{m_o c^2}{\lvert e\rvert} k_o \gamma_o \xi \eta^{1/2}$	$\gg \left(\frac{\sqrt{\pi}}{40}\xi^2\beta_{o\perp}^2\right)^{1/3}$
Case 3a: High Gain, $-Im(k)z \gg 1$ Collective, $\beta_{o\perp} \ll \beta_{crit}$, Dense-Cold Beam	$\frac{\sqrt{\gamma_{zo}}}{2}\xi^{1/2}\beta_{o\perp}k_o$	$\frac{\xi}{\gamma_{zo}}$	$\frac{m_o c^2}{\lvert e\rvert} k_o \gamma_o \xi^{1/2}\eta$	$\ll \eta$
Case 3b: High Gain, $-Im(k)z \gg 1$ Non-Collective, $\beta_{o\perp} \gg \beta_{crit}$, Dense-Cold Beam	$\frac{\sqrt{3}}{2^{4/3}}(\xi\beta_{o\perp})^{2/3}k_o$	$2^{-4/3}(\xi\beta_{o\perp})^{2/3}$	$\frac{m_o c^2}{\lvert e\rvert} k_o \gamma_o \xi \eta^{1/2}$	$\ll \eta$

The parameters are defined as: $\beta_{zo} = v_{zo}/c \approx 1$, $\xi = \frac{\omega_b/\sqrt{\gamma_o}}{ck_o}$, $k_o = 2\pi/l$, $\omega_b = \left(\frac{4\pi|e|^2 n_o}{m_o}\right)^{1/2}$, $\Omega_o = \frac{|e|B_o}{m_o c}$, $\beta_{o\perp} = \frac{\Omega_o/\gamma_o}{ck_o}$,

$\beta_{crit} = 4\left(\frac{\xi}{\gamma_{zo}^3}\right)^{1/2}$, $\gamma_o = (1 - \beta_{zo}^2 - \beta_{o\perp}^2)^{-1/2}$, $\gamma_{zo} = (1 - \beta_{zo}^2)^{-1/2}$, $E_o = (\gamma_o - 1)m_o c^2$, $E_{th} = \gamma_{zo}^2 \gamma_o m_o c V_{th}$, $\delta u_w/U_{th} = \frac{\sqrt{\pi}}{20}\xi^2\,\beta_{o\perp}^2 (E_o/E_{th})^3$.

Table II

Illustration of Visible Radiation Source ($\lambda_s = 0.58\ \mu m$)

(Strong Pump Scattering Regime)

Magnetic Pump Field Parameters

Pump Wavelength:	$l = 0.75cm$
Pump Magnetic Field Amplitude:	$B_0 = 7.5$ KG

Electron Beam Parameters

E-Beam Current:	$I_0 = 2kA$
E-Beam Energy ($\gamma_0 = 90$):	$E_0 = 45$ MeV
E-Beam Power:	$P_0 = 90$ GW
E-Beam Radius:	$r_0 = 0.1$ cm
Axial Beam Gamma:	$\gamma_{z0} = 80$
Energy Spread Due to Self Beam Potential:	$\Delta E/E_0 = 0.12\%$

Scattered Visible Radiation Parameters

Radiation Wavelength:	$\lambda_s = l/(2\gamma_{z0}^2) = 0.58\ \mu m$
e-Folding Length of Radiation:	$L_e = 28$ cm
Single Pass Efficiency:	$\eta = 0.25\%$
Radiation Power:	$P_s = 230$ MW

Table III — A Comparison of Experimental Studies of Stimulated Scattering from Relativistic Electron Beams

Scattering Regime	Experimental Configuration	Pump Wave	Electron Beam	Output Radiation	Performing Organization
1. Low Gain	Amplifier Filling Factor $= 2 \times 10^{-2}$	Magnetic Wiggler $l = 3.2$ cm $B_o = 2.4$ kG $L = 5.2$ m	24 MeV 0.07A, peak $n_o = 2 \times 10^9$ cm^{-3} $E_{th}/E_o = 0.1\%$	$\lambda_s = 10.6$ μm $G_L = 0.035$ (7% energy gain)	Stanford University (Elias et al, 1976)
2. Low Gain	Oscillator with Optical Cavity Mirror trans. = 1.5%	Magnetic Wiggler $l = 3.2$ cm $B_o = 2.4$ kG $L = 5.2$ m	43 MeV 2.6 A peak $E_{th}/E_o = .05\%$ .06 mm mrad	$\lambda_s = 3.4$ μm $\Delta\lambda_s/\lambda_s = 0.2\%$ 7 kW peak	Stanford University (Deacon et al, 1977)
3. High Gain, Collective	Superradiant Oscillator	Electromagnetic Wave $l = 2$ cm $\mathcal{E}_o = 4 \times 10^4$ V/cm $L = 0.36$ cm	2 MeV 30 kA peak $n_o = 3 \times 10^{12}$ cm^{-3} $\Delta E/E_o = 4\%$	$\lambda_s = 400$ μm $G_L > 2$ 1 MW peak	Naval Research Laboratory (Granatstein et al, 1977)
4. High Gain, Collective	Superradiant Oscillator	Magnetic Wiggler $l = 0.6$ cm $B_o = 0.5$ kG $L = 0.36$ m	0.86 MeV 5 kA peak $n_o = 3 \times 10^{11}$ cm^{-3} $\Delta E/E_o = 2\%$	$\lambda_s = 1500$ μm 8 MW peak	Columbia University (Marshall et al, 1977; Gilgenbach et al, 1978; and Gilgenbach, 1978)
5. High Gain, Collective	Oscillator with Optical Cavity Mirror trans. = 2%	Magnetic Wiggler $l = 0.8$ cm $B_o = 0.4$ kG $L = 0.4$ m	1.2 MeV 25 kA peak $n_o = 4 \times 10^{12}$ $\Delta E/E_o = 3\%$	$\lambda_s = 400$ μm $\Delta\lambda_s/\lambda_s = 2\%$ 1 MW peak	NRL and Columbia (McDermott et al, 1978)

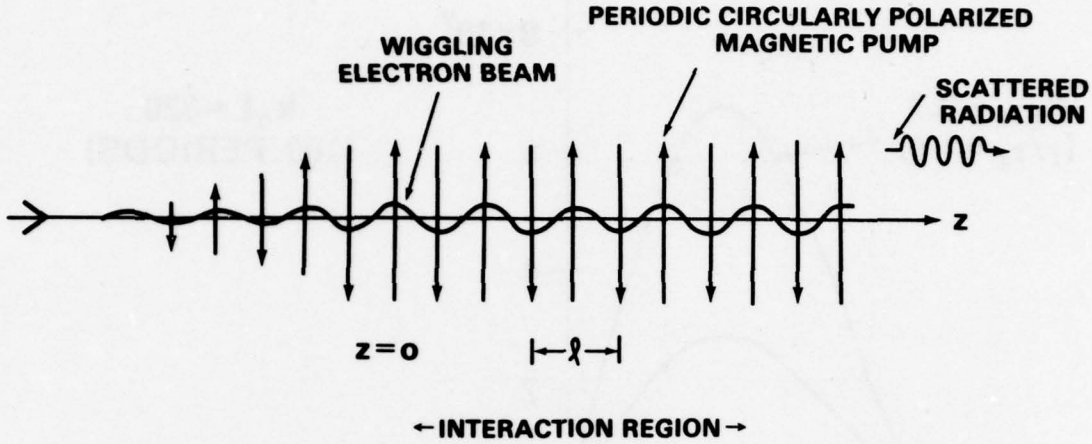

Figure 1 — Schematic of the free-electron laser model. The unmodulated electron beam enters the interaction region from the left. The pump field builds up adiabatically and reaches a constant amplitude for $z > 0$.

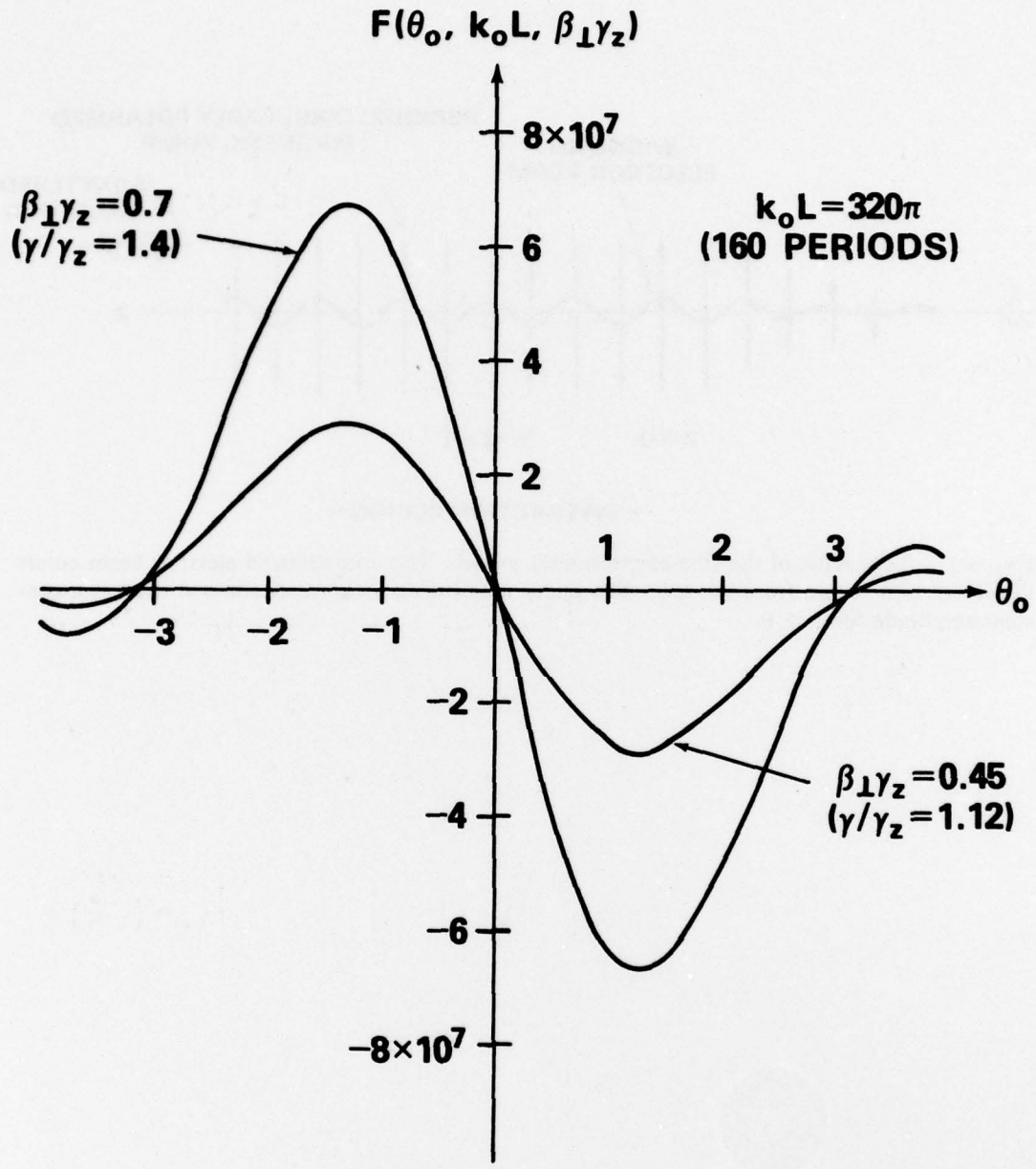

(a)

Figure 2 — The gain function $F(\theta_o, k_o L, \beta_\perp \gamma_z)$ corresponding to the low-gain, tenuous cold beam scattering limit. The interaction length for (a) is 160 pump periods and for (b) 1 pump period. Note that in (b) the slight asymmetry with respect to θ_o is due to the contributions of the terms $\sin^2\theta_o/\theta_o$ and $\sin^2(\theta_o + k_o L/2)/(\theta_o + k_o L/2)$.

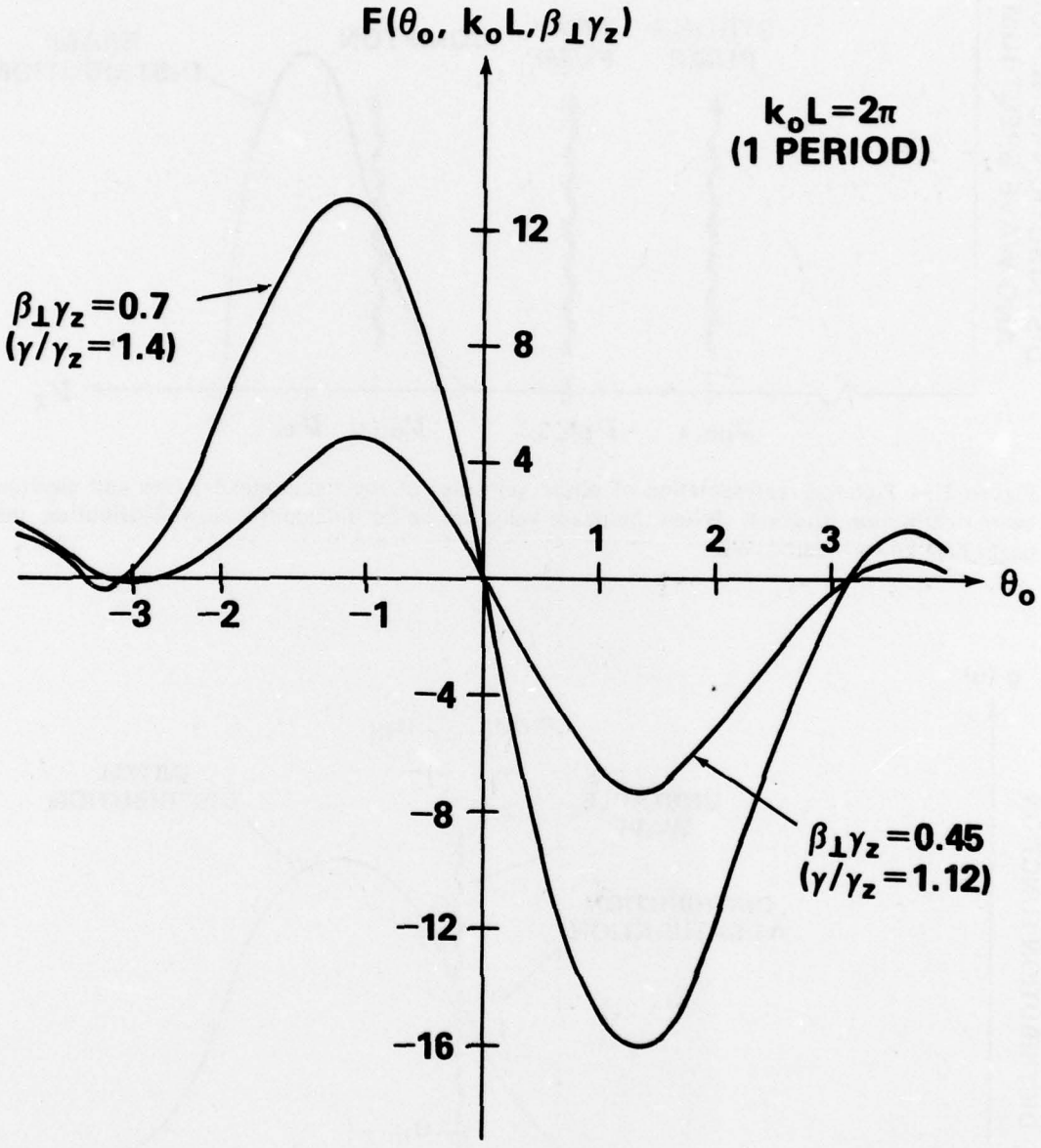

(b)

Figure 2 (Continued) — The gain function $F(\theta_o, k_oL, \beta_\perp \gamma_z)$ corresponding to the low-gain, tenuous cold beam scattering limit. The interaction length for (a) is 160 pump periods and for (b) 1 pump period. Note that in (b) the slight asymmetry with respect to θ_o is due to the contributions of the terms $\sin^2\theta_o/\theta_o$ and $\sin^2(\theta_o + k_oL/2)/(\theta_o + k_oL/2)$.

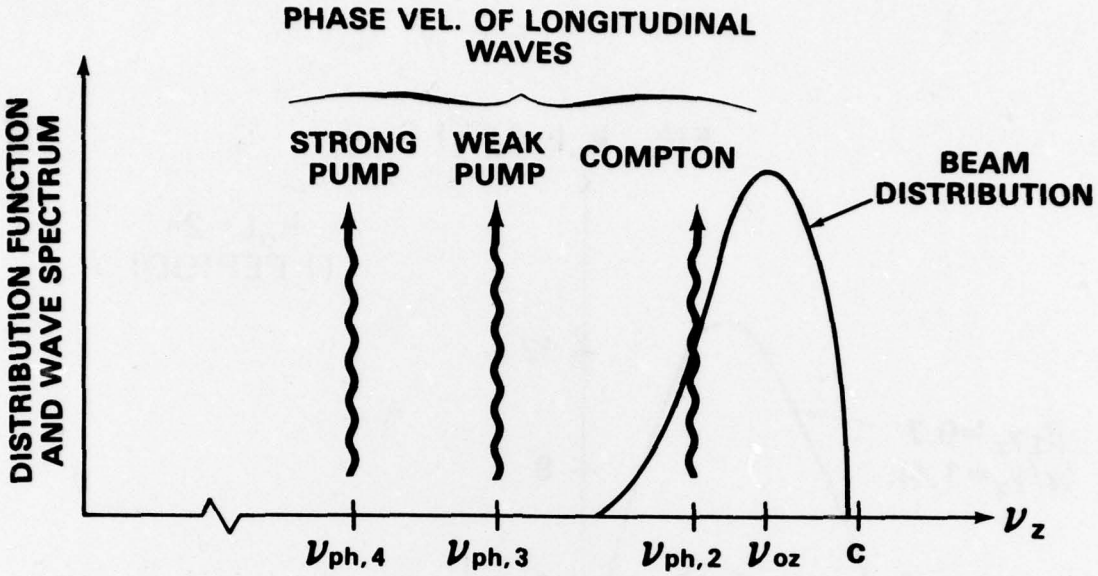

Figure 3 — Pictorial representation of phase velocities of the longitudinal waves and electron beam distribution function. When the phase velocities lie far outside the beam distribution, the beam may be considered cold.

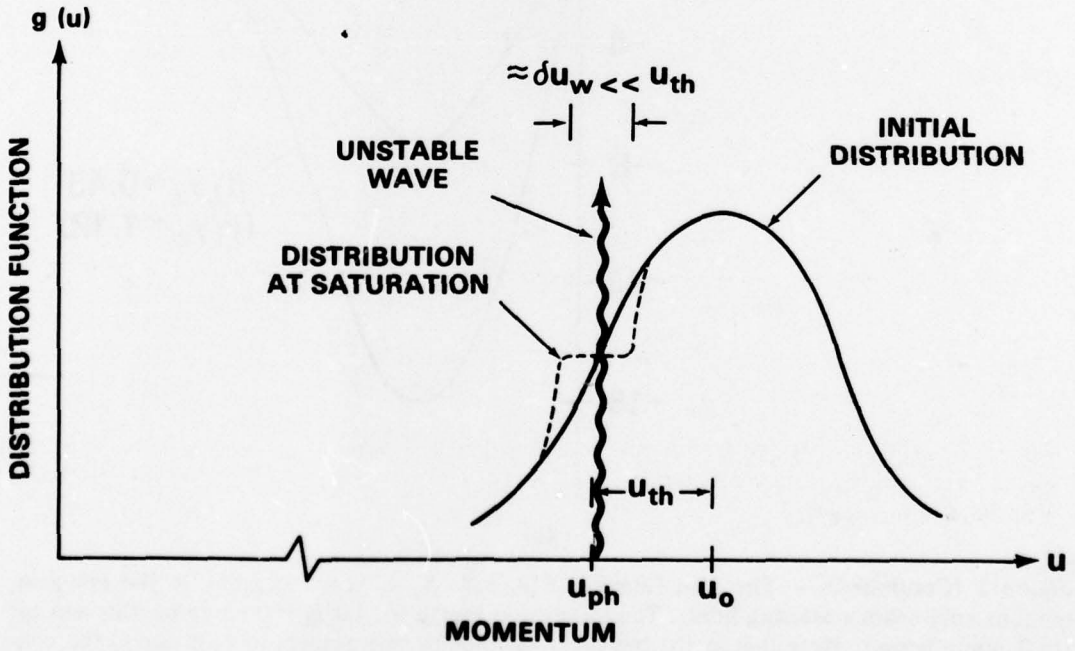

Figure 4 — Schematic of quasilinear plateau formation in saturation of relativistic stimulated Compton scattering limit.

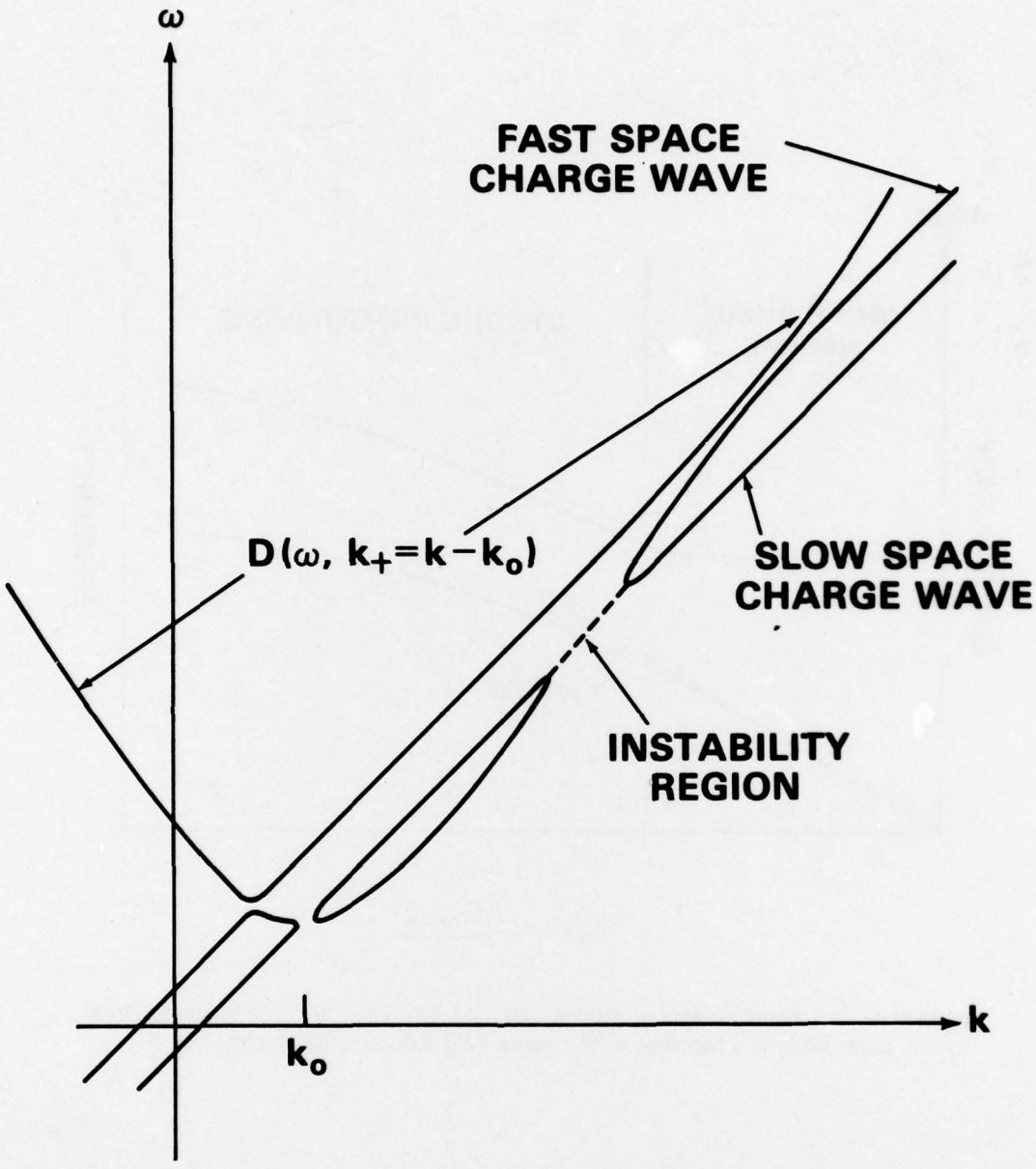

Figure 5 — Coupled dispersion diagrams of the beam waves and transverse electromagnetic waves. Instability occurs near the intersection between the slow beam made and transverse electromagnetic made.

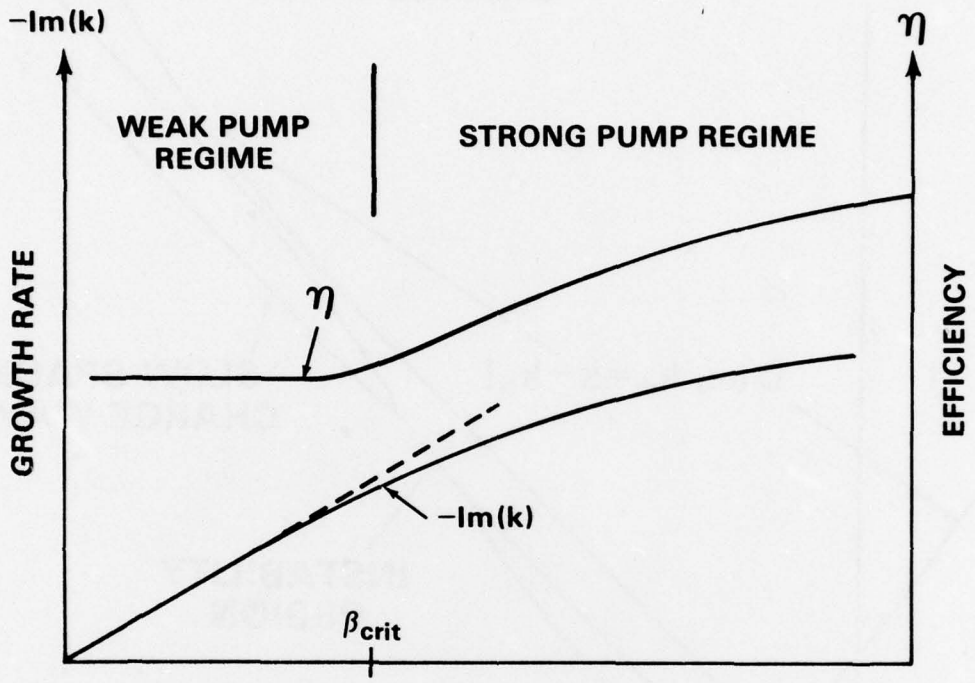

$$\beta_{o\perp} = \frac{\Omega_o/\gamma_o}{c\,k_o}$$

Figure 6 — Schematic of spatial growth rate and efficiency in the high-gain, dense cold beam limit as a function of the pump field strength characterized by $\beta_{o\perp}$.

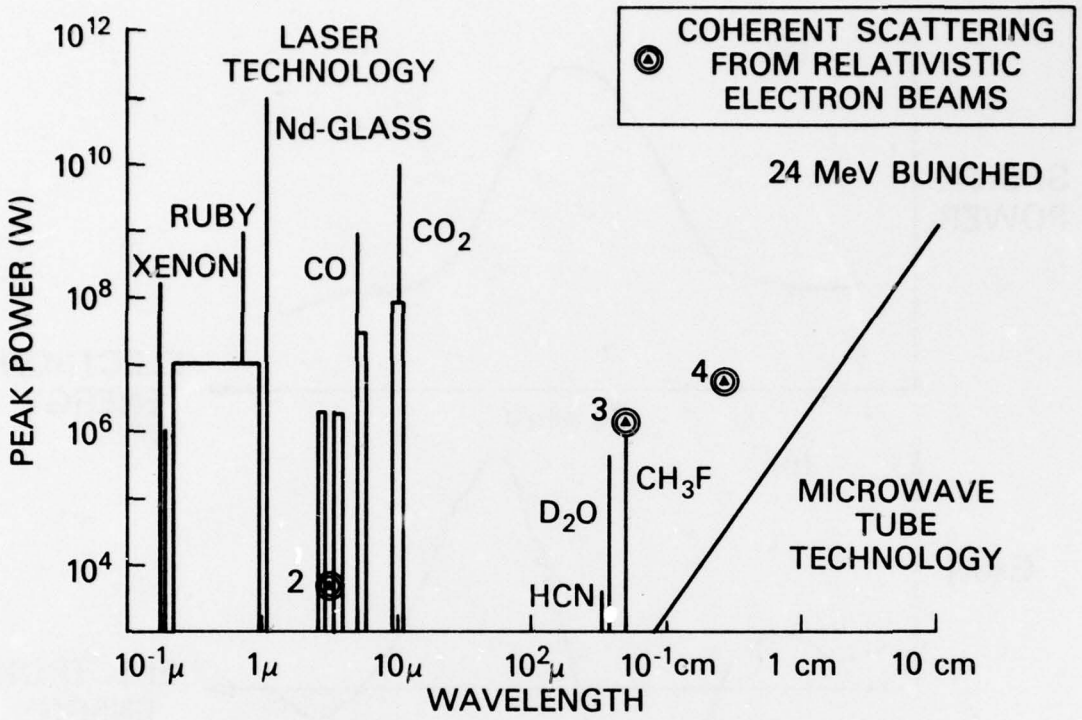

Figure 7 — A Comparison of Technologies Available for the Generation of High-Power Coherent Radiation. The three data points correspond to the preliminary coherent scattering results and are numbered as in Table III.

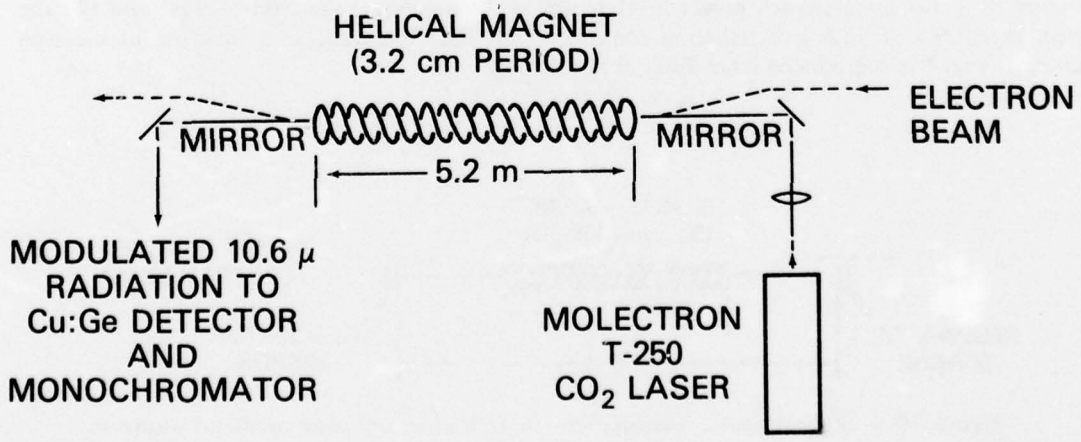

Figure 8 — Experimental arrangement in free electron amplifier study in the low-gain regime. Fig. 8 is reproduced from Elias et al (1976).

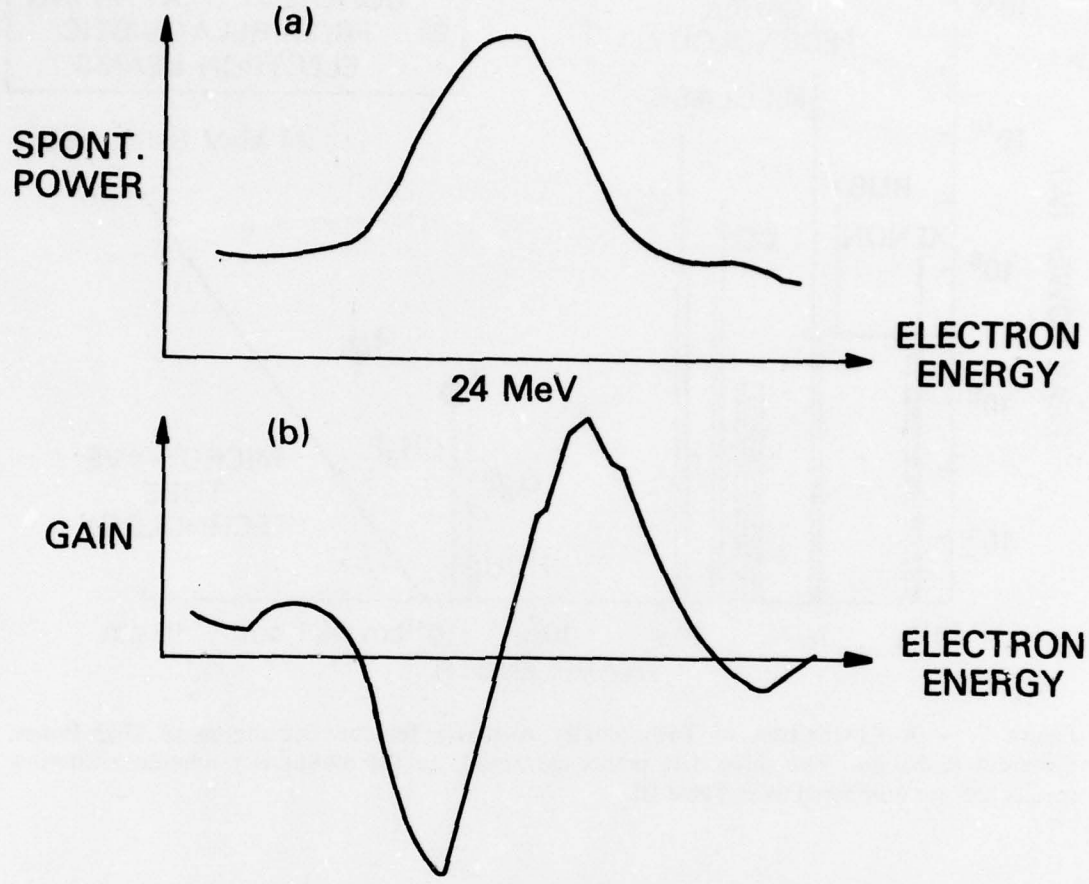

Figure 9 — (a) Spontaneous power at 10.6 μm as a function of electron energy, and (b) the gain in energy of 10.6 μm radiation imposed from the CO_2 laser as a function of electron energy. Fig. 9 is reproduced from Elias et al (1976).

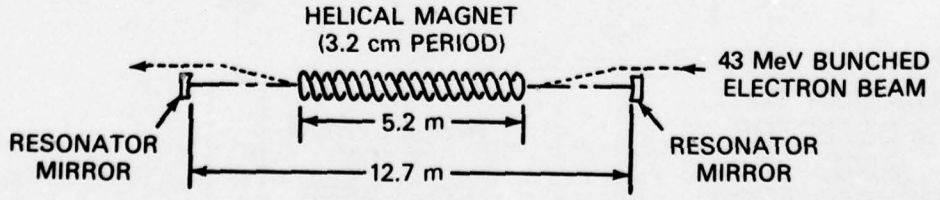

Figure 10 — Experimental arrangement in free electron laser oscillator study in the low-gain regime. Fig. 10 is reproduced from Deacon et al (1977).

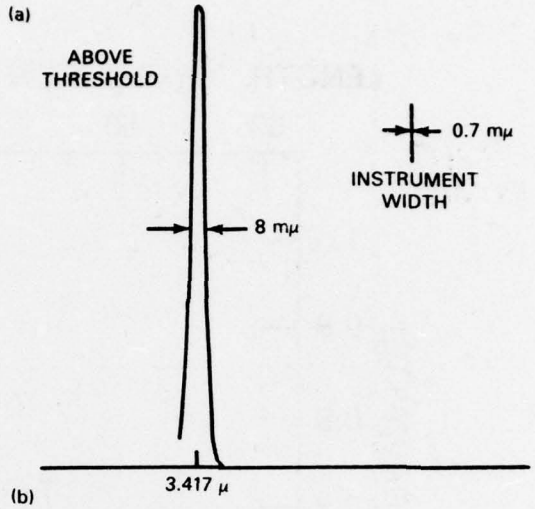

Figure 11 — Emission spectra of laser oscillator (a) above lasing threshold (b) spontaneous radiation emitted by electron beam. Fig. 11 is reproduced from Deacon et al., (1977).

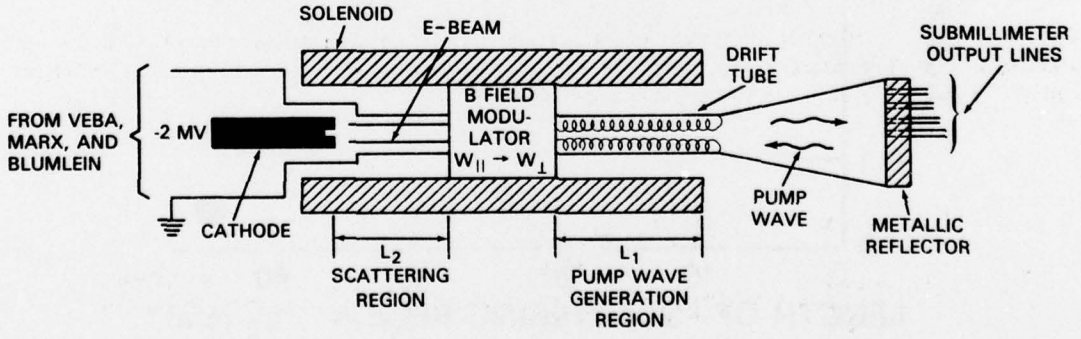

Figure 12 — Experimental arrangement in study of stimulated scattering in the high-gain, collective regime with electromagnetic pump wave (Granatstein et al, 1977). The VEBA electron accelerator system is described in Parker and Ury (1975).

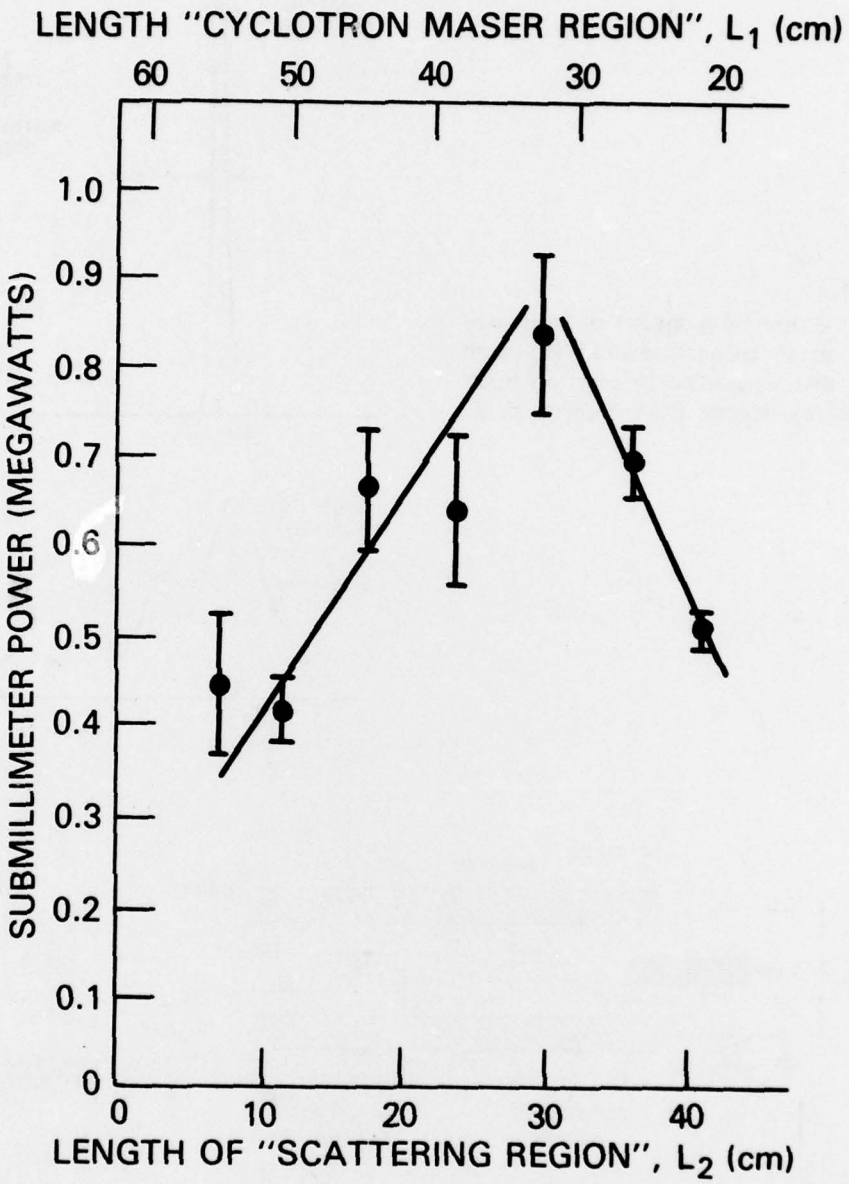

Figure 13 — Radiated power at 400 μm vs. length of scattering region (Granatstein et al, 1977).

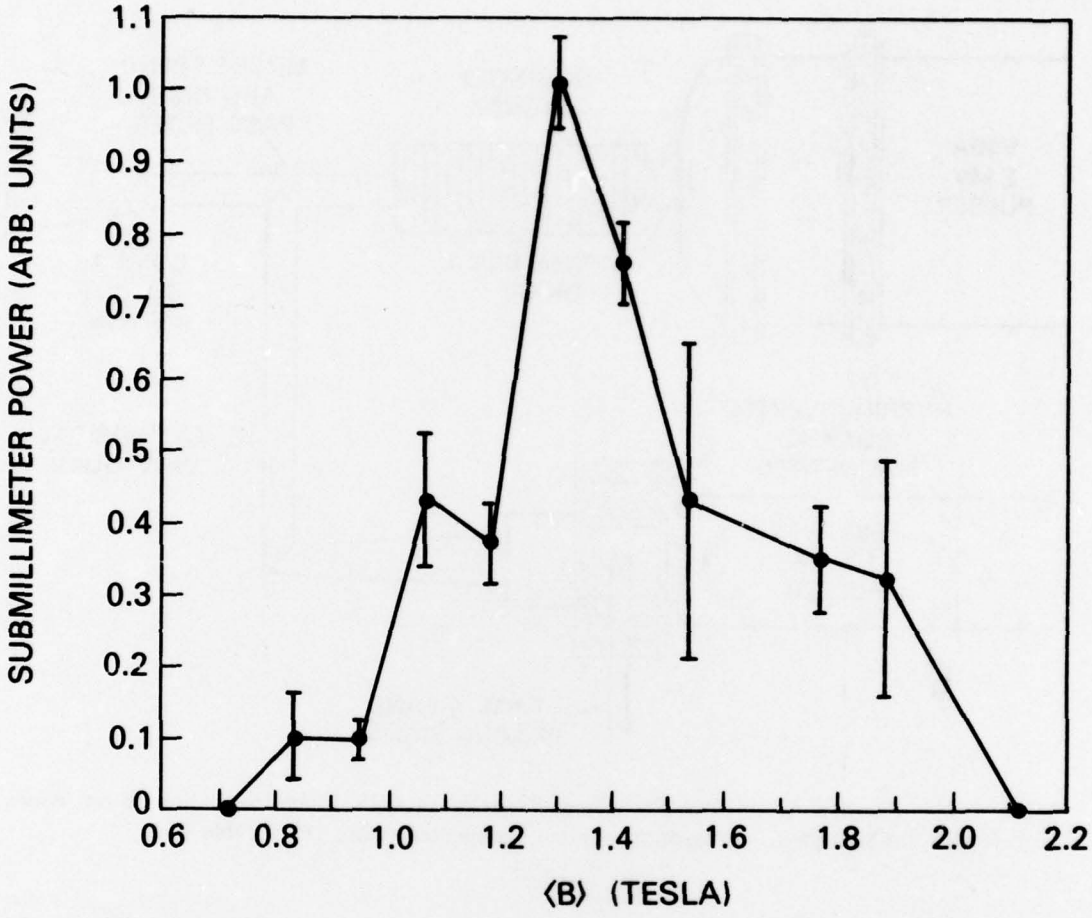

Figure 14 — Submillimeter output radiation at 400 μm vs. strength of uniform axial magnetic field (Granatstein, et al, 1977).

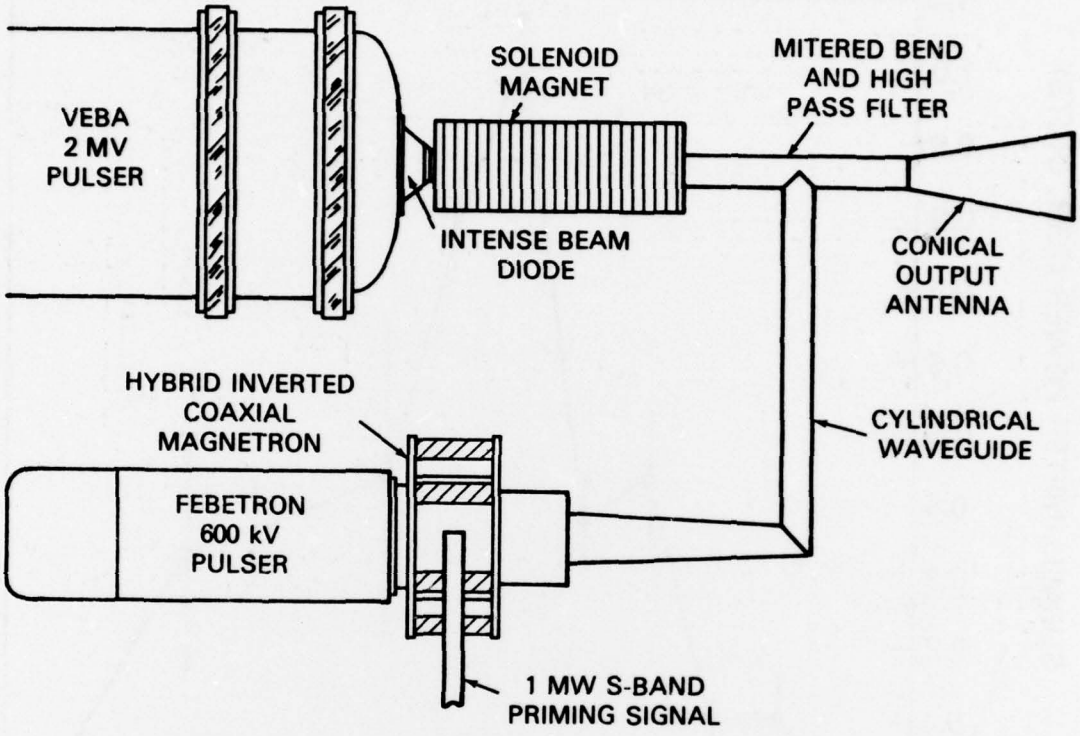

Figure 15 — Planned Stimulated Scattering Experiment with Electromagnetic Pump Wave. Operation in the high-gain, strong-pump regime is expected (Case 3b in Table I).

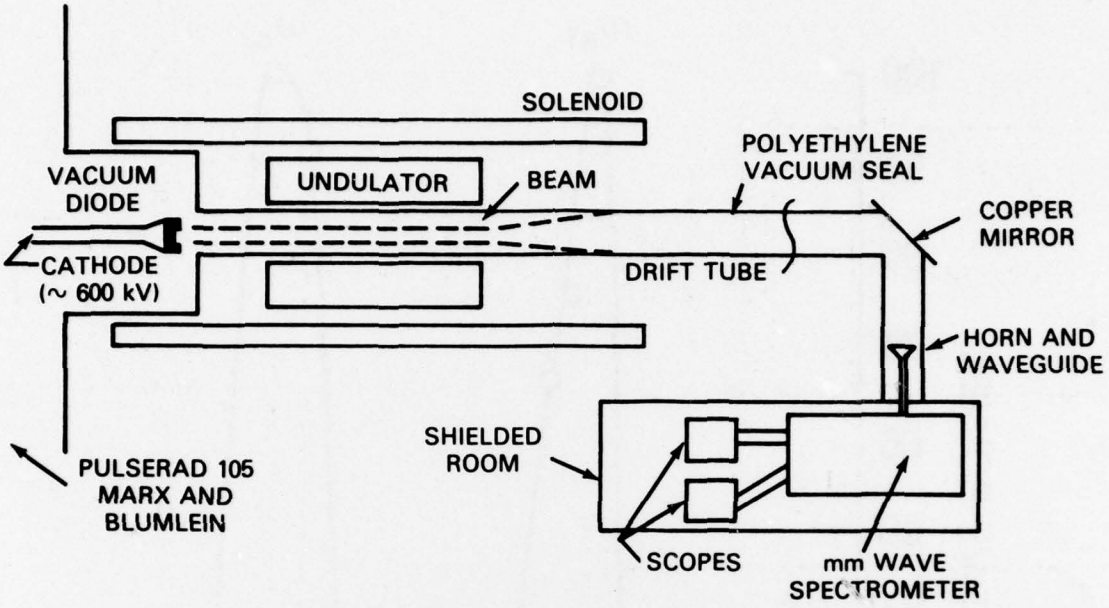

Figure 16 — Experimental arrangement in study of stimulated scattering in the high-gain, collective regime with magnetic undulator pump. Fig. 16 is reproduced from Gilgenbach et al (1978).

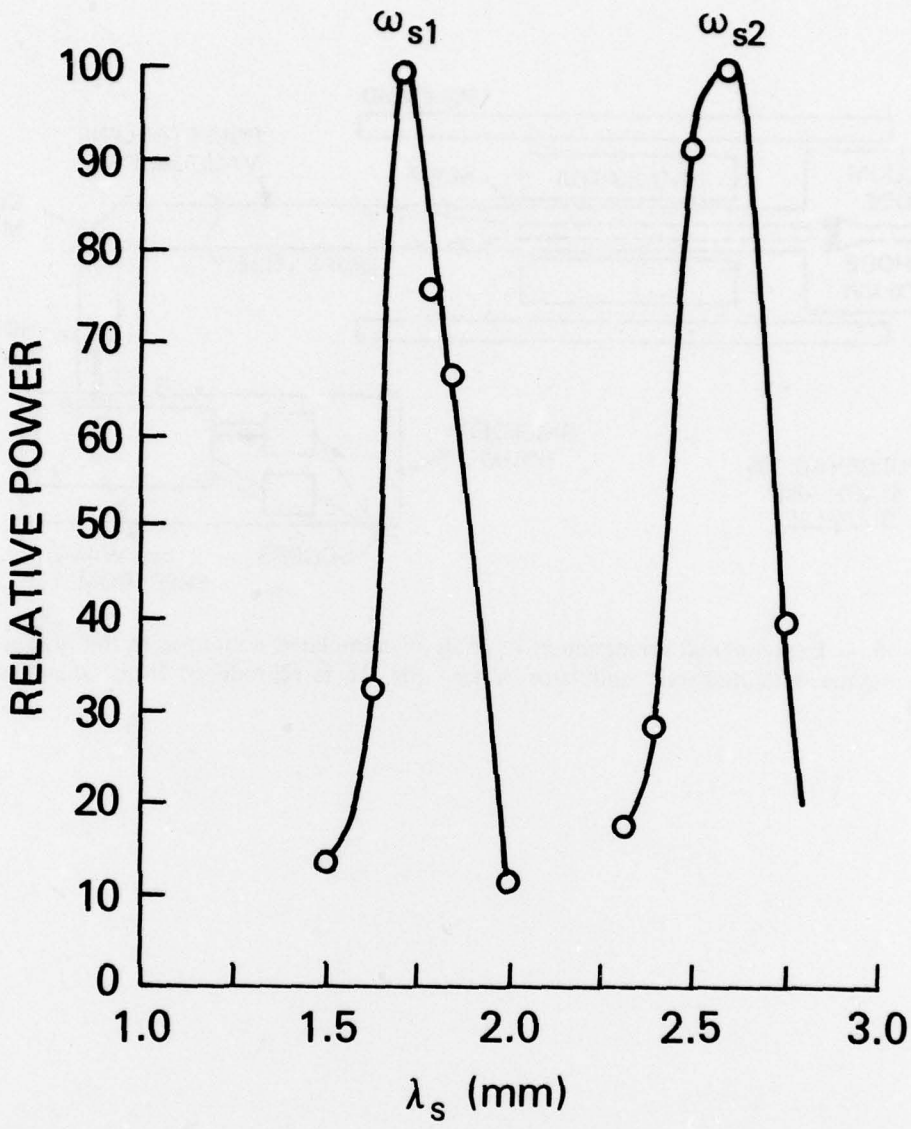

Figure 17 — Spectrum of output radiation. Each peak arbitrarily normalized to 100 on vertical scale. $l = 8$ mm, $\gamma_{zo} = 1.8$, $<B> = 7.6$ kG for peak at ω_{S2}, $n_o = 3 \times 10^{11}\text{cm}^{-3}$. Fig. 17 is reproduced from Gilgenbach et al., (1978).

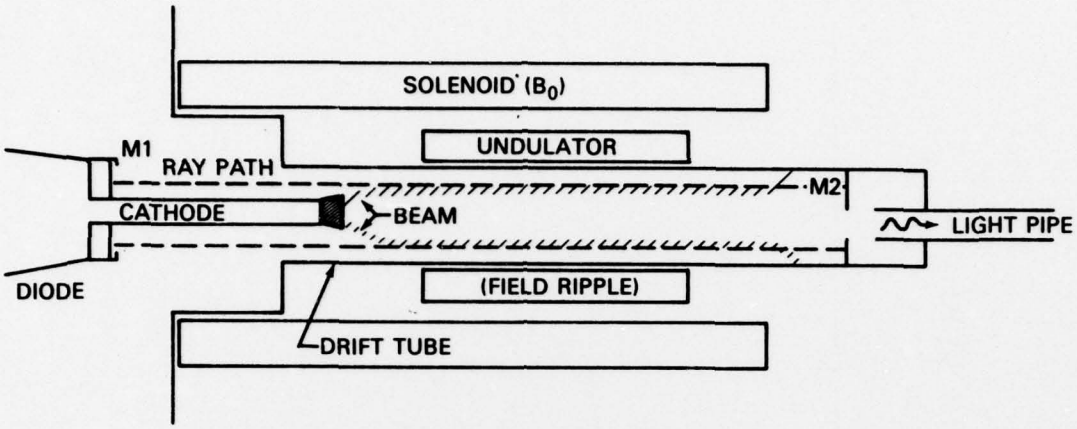

Figure 18 — Experimental arrangement in study of high-gain free electron laser with quasi-optical cavity. M_1 and M_2 designate mirrors. Fig. 18 is reproduced from McDermott et al (1978).

*U.S. GOVERNMENT PRINTING OFFICE: 1978 281-484/192 1-3